Journal of Medicinal Chemistry

Article

pubs.acs.org/jmc

ent-Kaurane Diterpenoids from Chinese Liverworts and Their Antitumor Activities through Michael Addition As Detected in Situ by a Fluorescence Probe

Zhaomin Lin,[†,§] Yanxia Guo,[‡,§] Yanhui Gao,[†] Shuqi Wang,[†] Xiaoning Wang,[†] Zhiyu Xie,[†] Huanmin Niu,[‡] Wenqiang Chang,[†] Lei Liu,[†] Huiqing Yuan,[‡] and Hongxiang Lou*[,†]

[†]Department of Natural Products Chemistry, Key Laboratory of Chemical Biology of Ministry of Education, School of Pharmaceutical Sciences, Shandong University, No. 44 West Wenhua Road, Jinan 250012, People's Republic of China

[‡]Department of Biochemistry and Molecular Biology, School of Medicine, Shandong University, No. 44 West Wenhua Road, Jinan 250012, People's Republic of China

Supporting Information

ABSTRACT: It is generally accepted that the origin of the cytotoxicity of *ent*-kaurane diterpenoids is due to the formation of reactive oxygen species (ROS) and that the α,β-unsaturated carbonyl is a pivotal moiety. Herein we demonstrate the isolation of 32 new and 12 known *ent*-kaurane diterpenoids from two Chinese liverworts. These compounds and three semisynthesized derivatives were screened against human cancer cell lines. The results revealed that their anticancer activities are caused by ROS formation through Michael modification of the protein thiols and depletion of glutathione unselectively. We also found that *N*-acetylcysteine reverses the cytotoxicity of these diterpenoids by forming Michael adducts, not through a well-recognized ROS scavenging pathway as previously reported. In situ intracellular thiol detection helped us visualize the intracellular distribution of the diterpenoids and determine the potency of their cytotoxicity. An alkaline analogue was found to be more selective because of the altered subcellular distribution.

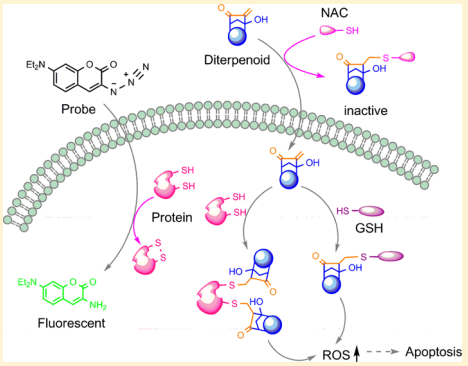

INTRODUCTION

Natural products have a profound impact upon both chemical biology and drug discovery, and the great structural diversity of natural products with various interesting biological characteristics has always provided medicinal chemists an important source of inspiration in their search for new molecular entities with pharmacological activities.[1−3] Among them, *ent*-kaurane diterpenoids are remarkable chemical markers in both liverworts[4−8] and some other higher plants.[9−11] They exhibit considerable pharmacological activities, including antitumor, antituberculosis, antibacterial, and anti-inflammatory effects.[11−13] Some of them have recently been developed into cancer therapeutic agents.[14,15] The widely accepted mechanism for these anticancer agents is the Michael addition of soft nucleophiles, such as thiols and protein sulfhydryl groups, onto the α,β-unsaturated ketone moiety, leading to the deactivation of SH enzymes or SH coenzymes.[16−18] Despite some progress, the poor selectivity has restricted the development of these diterpenoids into drugs, which may be ascribed to the poor selected intracellular distribution and multitargeting.[11] The diversity of the diterpenoids provides us a good opportunity to explore the structure−activity relationship (SAR), the intracellular distribution, and the target molecules to improve the state of art of the area.

In this work, a small library of *ent*-kaurane diterpenoids was built by ongoing chemical investigations on the Chinese liverworts *Jungermannia fauriana* and *Jungermannia hyalina* in our laboratory.[19−22] Twenty new (**1**−**20**) and four known (**21**−**24**) *ent*-kaurane diterpenoids from the liverwort *J. fauriana* and 12 new (**25**−**36**) and 11 known (**22**−**24** and **37**−**44**) structures from *J. hyalina* (Figure 1) were isolated separately, and three *ent*-kaurane derivatives (**45**−**47**) were semisynthesized from stevioside (Scheme 1).[23] Herein we report the discovery of new *ent*-kaurane diterpenoids and their cytotoxic effects on human cancer cell lines. The relationship between selectivity and intracellular distribution as detected by our developed in situ imaging method was investigated. A possible way to improve the selectivity to kill cancer cells by altering the drug subcellular distribution was also preliminarily explored.

RESULTS AND DISCUSSION

Structure Elucidation. The EtOH extract of *J. fauriana* was repeatedly chromatographed over MCI gel, silica gel, Sephadex LH-20, and further semipreparative HPLC to yield 20 new (**1**−**20**) and four known (**21**−**24**) *ent*-kaurane diterpenoids. By a

Received: February 4, 2015

DOI: 10.1021/acs.jmedchem.5b00208
J. Med. Chem. XXXX, XXX, XXX−XXX

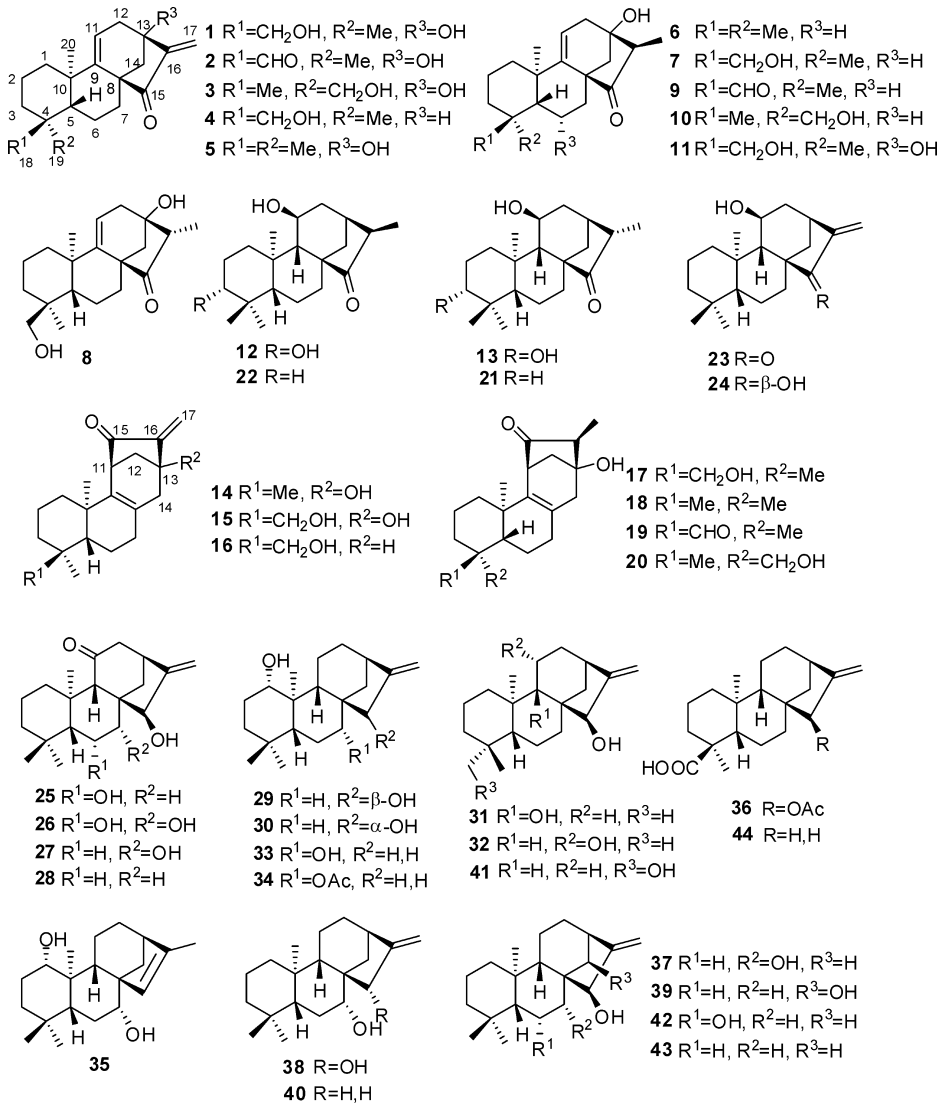

Figure 1. Structures of compounds **1**–**24** isolated from the liverwort *J. fauriana* and compounds **22**–**44** from the liverwort *J. hyalina*.

similar method, 12 new (**25**–**36**) and 11 known (**22**–**24** and **37**–**44**) diterpenoids were isolated from *J. hyalina*.

Compound **1**, isolated as colorless crystals (MeOH), was assigned the molecular formula $C_{20}H_{28}O_3$ on the basis of the NMR data and an $[M + NH_4]^+$ ion at *m/z* 334.2375 (calcd 334.2377) found by high-resolution electrospray ionization mass spectrometry (HR-ESI-MS), which indicated seven indices of hydrogen deficiency. The IR spectrum showed absorption bands of hydroxyl (3390 cm^{-1}) and carbonyl (1722 cm^{-1}) groups. The ^1H NMR spectrum of **1** (Table S1 in the Supporting Information) displayed signals for two tertiary methyl groups at δ_H 0.84 (s) and 1.13 (s), a pair of oxygenated methylene protons at δ_H 3.50 (d, J = 11.4 Hz) and 3.04 (d, J = 11.4 Hz), an olefinic proton at δ_H 5.55 (t, J = 3.0 Hz), and an exocyclic methylene at δ_H 6.03 (s) and 5.64 (s). The ^{13}C NMR data (Table S5), analyzed with the help of heteronuclear single-quantum correlation (HSQC) data, indicated that 20 carbons of **1** are two methyls, nine methylenes, two methines, and seven quaternary carbons. The aforementioned spectral data allowed the assignment of an *ent*-kaurane diterpenoid skeleton.[24−26] In the heteronuclear multiple-bond correlation (HMBC) spectrum (Figure S1 in the Supporting Information), the long-range correlations of CH_3-20 (δ_H 1.13) with C-9 (δ_C 150.2) and C-10 (δ_C 38.7) and of the olefinic proton H-11 (δ_H 5.55) with C-10 (δ_C 38.7), C-12 (δ_C 43.0), and C-13 (δ_C 74.4) confirmed the double bond between C-9 and C-11. The HMBC correlations of H_2-17 (δ_H 6.03 and 5.64) with C-12, C-13, and C-15 (δ_C 201.8) revealed the presence of the oxygenated quaternary carbon at C-13. Both the oxygenated methylene (δ_H 3.50 and 3.04) and the methyl at δ_H 0.84 showed HMBC correlations to C-3 (δ_C 35.2), C-4 (δ_C 38.2), and C-5, which assigned the location of the hydroxyl group at C-18 or C-19. The nuclear Overhauser effect spectroscopy (NOESY) correlations of the oxygenated methylene to H-5 (δ_H 1.73) and H-6β (δ_H 1.98–2.08) and of the methyl at δ_H 0.84 to CH_3-20 (δ_H 1.13) (Figure S1) suggested that the hydroxyl group is at C-18 and the α-CH_3 at C-4. To determine the absolute configuration, compound **1** was subjected to single-crystal X-ray diffraction analysis with Cu Kα radiation, which unambiguously confirmed the structure and the depicted absolute configuration to be that of an *ent*-kaurane diterpenoid (Figure S2). Accordingly, **1** was elucidated as 13,18-dihydroxy-*ent*-9(11),16-kauradien-15-one.

The same strategy was used to determine the structures of the new compounds **2**–**20** and **25**–**36** as shown in Figure 1 (for the detailed elucidation, see the Supporting Information). The known compounds were identified by comparison of their

DOI: 10.1021/acs.jmedchem.5b00208
J. Med. Chem. XXXX, XXX, XXX−XXX

Scheme 1. Synthesis of Stevioside Derivatives 45−47[a]

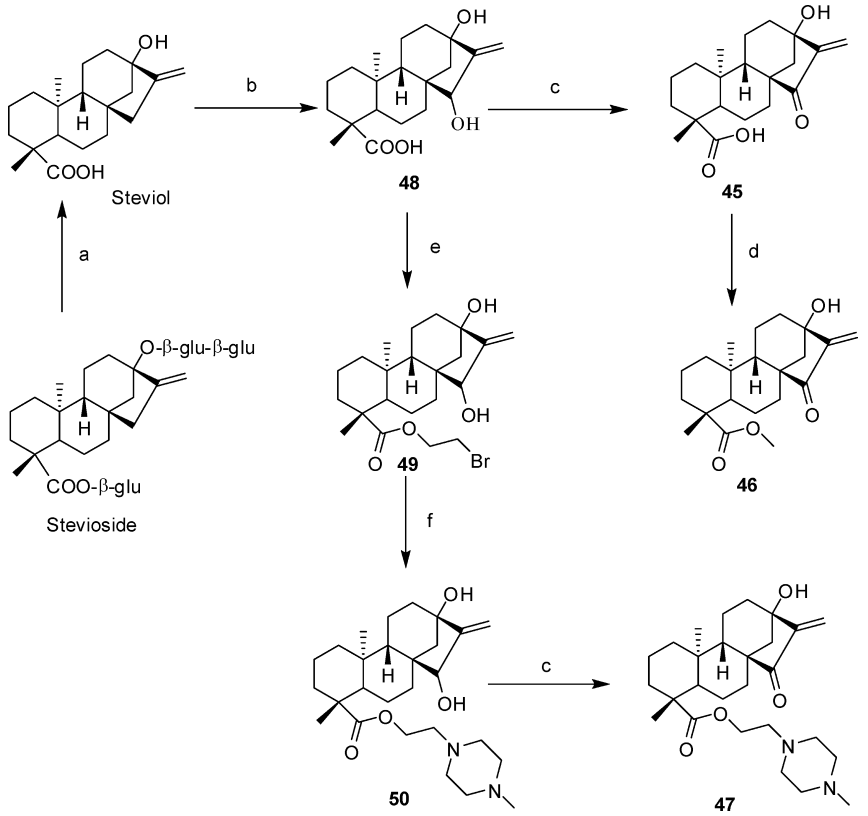

[a]Reagents and conditions: (a) $NaIO_4$, H_2O, room temperature, 16 h; KOH, H_2O, reflux, 1 h. (b) SeO_2, *t*-BuOOH, THF, room temperature, 20 h. (c) PDC, DMF, room temperature, 12 h. (d) CH_3I, DMF, room temperature, 8 h. (e) $BrCH_2CH_2Br$, K_2CO_3, DMF, room temperature, 4 h. (f) *N*-methylpiperazine, DMF, reflux, 10 h.

NMR and MS data with reported data (see the Supporting Information for details).

In Vitro Antiproliferation Activity. Cytotoxicity screening of the diterpenoid library against 13 human cancer cell lines indicated that compounds **1**−**5**, **14**−**16**, **23**, and **45**−**47**, which contain an *exo*-methylene cyclopentanone system, possess strong activity, while all of the other compounds are inactive (IC_{50} > 50 μM) (Table 1). The screening results also suggested that the active compounds showed comparable cytotoxic activities against cancer and normal cell lines, revealing poor selectivity with a low selectivity index (SI). An SAR investigation (Figure 2) showed that the *exo*-methylene cyclopentanone system in the D ring is pivotal for the cytotoxicity. Any destruction of this system, e.g., by saturation of the methylene group (compounds **6**−**13**, **17**−**22**, and **24**) or the ketone group (compounds **25**−**44**) led to complete loss of cytotoxicity. Comparison of the IC_{50} values of **1** and **15** with those of **4** and **16** indicates that the C13-OH should be beneficial to the cytotoxicity. Moreover, compounds with a hydroxyl group at C-11 (e.g., **23**) also showed increased activity. However, compounds **1** and **3**, analogues of **5** bearing a hydroxyl group on the methyl group at C-4, proved to be less potent (5.5 μM for **1** and 6.6 μM for **3**) than compound **5** (3.2 μM) against the PC3 cell line. The activity further decreased upon oxidation of the hydroxymethyl group to a formyl group (**2**, 11.4 μM) or a carboxylic acid (**45**, 30.1 μM), although the loss of activity could be partially reversed by esterification of the carboxylic acid (**46**, 6.1 μM). Comparison of the activities of **5** and **14** suggests that rearrangement of the D ring in the *ent*-kaurane diterpenoid skeleton has no significant effect on the efficacy.

ROS-Induced Cell Death by Diterpenoids. Reactive oxygen species (ROS) can modulate the activities and expressions of many transcription factors and signaling proteins that are involved in stress response and cell survival through multiple mechanisms.[27−29] Compounds that promote ROS generation in cancer cells show promising anticancer activity.[30−33] The *ent*-kaurane-type diterpenoids oridonin and adenanthin were reported to interact with thioredoxin/thioredoxin reductase[34] in acute myeloid leukemia or peroxiredoxin I and II[18] in acute promyelocytic leukemia through increased intracellular ROS, which in turn induces apoptotic cell death or cell differentiation. However, in their research, the role of induced ROS was unintentionally wrongly designed using *N*-acetylcysteine (NAC) as an antioxidant to reverse the ROS-initiated apoptosis.[18,34]

To investigate whether ROS are involved in cell death induced by our compounds, we measured cellular changes in the ROS levels after treatment with the test diterpenoid **46** using the ROS-sensitive fluorometric probe 2′,7′-dichlorofluorescein diacetate (DCFH-DA). As expected, **46** elevated the ROS levels of treated cells in a time-dependent manner (Figure 3A,B). NAC, a ROS scavenger, dramatically diminished the **46**-induced ROS level and significantly attenuated the inhibitory effect of **46** on cell viability (Figure 3A,C), which was consistent with literature reports.[18,34] However, NAC possesses a mercapto moiety, which has the potential to react with the α,β-unsaturated carbonyl moiety of diterpenoids. To verify this

DOI: 10.1021/acs.jmedchem.5b00208
J. Med. Chem. XXXX, XXX, XXX−XXX

Table 1. Cytotoxicities of Compounds 1−47 against Various Human Cancer Cell Lines[a]

compd[b]	PC3	DU145	LNCaP	RWPE1	MDA-MB231	NCI-H1299	SKOV3	LOVO	T24	K562	HL-60	SH-SYSY	A172	Saos-2
1	5.5 ± 0.1	6.3 ± 0.5	11.6 ± 1.0	11.7 ± 1.3	12.3 ± 1.1	10.7 ± 0.8	8.6 ± 0.4	9.0 ± 0.6	10.4 ± 1.0	10.2 ± 0.1	3.7 ± 0.2	4.4 ± 0.1	4.4 ± 0.3	7.8 ± 0.2
2	11.4 ± 1.0	11.6 ± 0.7	9.5 ± 0.4	12.7 ± 0.5	21.6 ± 0.7	12.2 ± 0.7	7.4 ± 0.7	9.3 ± 0.9	5.9 ± 0.7	6.3 ± 0.7	4.4 ± 0.7	4.2 ± 0.5	4.4 ± 0.5	7.3 ± 0.6
3	6.6 ± 0.7	8.3 ± 0.3	12.8 ± 0.2	13.2 ± 0.3	15.5 ± 0.9	19.0 ± 1.1	11.3 ± 0.5	18.4 ± 1.1	13.2 ± 0.2	10.4 ± 1.1	6.7 ± 0.5	4.9 ± 0.2	13.0 ± 0.9	15.8 ± 0.9
4	21.5 ± 1.2	31.0 ± 2.2	16.3 ± 1.0	39.3 ± 2.0	32.0 ± 1.8	14.5 ± 0.5	22.3 ± 1.9	11.2 ± 0.9	17.7 ± 1.4	13.8 ± 0.5	4.7 ± 0.2	9.8 ± 0.4	20.3 ± 1.0	14.0 ± 1.2
5	3.2 ± 0.2	5.5 ± 0.3	3.2 ± 0.2	6.2 ± 0.1	4.2 ± 0.5	2.4 ± 0.1	1.8 ± 0.2	1.8 ± 0.1	1.7 ± 0.2	1.9 ± 0.1	1.0 ± 0.1	1.2 ± 0.1	3.8 ± 0.3	1.3 ± 0.1
14	2.2 ± 0.1	3.2 ± 0.2	2.8 ± 0.1	6.3 ± 0.1	3.4 ± 0.3	2.6 ± 0.1	2.9 ± 0.1	2.3 ± 0.1	2.3 ± 0.1	2.2 ± 0.1	1.9 ± 0.1	1.6 ± 0.1	2.7 ± 0.1	2.4 ± 0.1
15	8.2 ± 0.3	9.4 ± 1.0	NT[d]	18.6 ± 0.1	10.4 ± 0.4	NT	NT	NT	NT	NT	NT	NT	NT	NT
16	–[c]	–	–	–	–	–	–	35.2 ± 2.7	49.1 ± 3.5	41.7 ± 2.8	23.6 ± 2.4	33.8 ± 2.9	–	35.5 ± 2.0
23	1.9 ± 0.2	4.5 ± 0.1	2.5 ± 0.2	5.2 ± 0.1	4.8 ± 0.4	2.6 ± 0.2	1.7 ± 0.1	1.4 ± 0.1	2.1 ± 0.1	1.5 ± 0.1	0.9 ± 0.1	0.7 ± 0.1	3.2 ± 0.2	1.4 ± 0.1
45	30.1 ± 0.5	48.5 ± 3.3	NT	27.0 ± 2.4	37.2 ± 1.4	32.8 ± 2.9	NT	NT	NT	9.9 ± 0.3	7.9 ± 0.5	NT	NT	NT
46	6.1 ± 0.1	10.8 ± 1.7	NT	7.0 ± 1.1	5.2 ± 1.0	9.2 ± 0.7	NT	NT	NT	2.9 ± 0.5	1.5 ± 0.1	NT	NT	NT
47	8.2 ± 0.2	14.9 ± 0.9	NT	29.3 ± 0.7	27.5 ± 0.6	10.9 ± 0.2	NT	NT	NT	4.1 ± 0.2	3.0 ± 0.1	NT	NT	NT
cisplatin[e]	19.9 ± 0.4	29.2 ± 0.6	27.5 ± 0.7	33.8 ± 2.0	20.2 ± 1.0	21.9 ± 0.9	17.5 ± 0.8	19.5 ± 0.7	15.7 ± 0.6	20.2 ± 0.8	21.5 ± 0.9	12.5 ± 0.4	15.2 ± 0.8	18.5 ± 0.8

[a]Results are expressed as the mean IC_{50} ± standard deviation (SD) in μM. [b]All of the other compounds were inactive (IC_{50} > 50 μM) toward all of the selected cell lines. [c]Not active (IC_{50} >50 μM). [d]Not tested. [e]Cisplatin was used as the positive control. The experiments were performed three times.

hypothesis, we first obtained the conjugated compound **46**−**NAC** by incubating **46** with NAC. Then we detected the probable reaction after addition of **46** to medium containing NAC by HPLC−MS/MS. As shown in Figure 3D, blank cell culture medium, medium with 5 mM NAC, and medium with 10 μM **46** were used as controls, and the conjugated product **46**−**NAC** was easily detected in the medium when NAC was added to the test medium containing **46**. Meanwhile, the prototype compound **46** was hardly detected. These results indicate that NAC reverses the cytotoxicity of diterpenoids not through ROS scavenging but rather through reaction with the compounds that results in loss of efficacy. The end-conjugated product is not toxic to cancer cells (IC_{50} > 50 μM). Therefore, it is not correct to use NAC as an antioxidant to investigate the role of ROS in cell death of such diterpenoids.[18,34−37]

Glutathione (GSH), a thiol-based intracellular antioxidant, is a major ROS scavenging agent in cells.[38] Depletion of GSH would result in ROS accumulation and cell death.[39,40] Again using compound **46**, we detected its effect to decrease the level of cellular GSH. The results showed that the GSH content in the PC3 cells was reduced upon treatment with **46** in a time-dependent manner (Figure 4A). Meanwhile, the levels of GSSG (the oxidized form GSH) decreased after a slight increase, and the total cellular glutathione (GSH + GSSG) decreased in a time-dependent manner. It is noteworthy that GSH is the most abundant intracellular non-protein sulfhydryl-containing compound. As we have demonstrated that **46** can react with the sulfhydryl group of NAC, we supposed that the compound might also react with GSH. As expected, conjugated **46**−**GSH** was distinctly detected in the treated cells by HPLC−MS/MS, as shown in Figure 4B. The antioxidant function of GSH is accomplished largely by the redox cycle of GSH and GSSG.[40] Because of the formation of the carbon−sulfur bond, the activity of GSH cannot be restored, resulting in a decrease of the content of both GSH and GSSG. Collectively, these results clearly demonstrate that **46** depletes intracellular GSH through a conjugation reaction.

In Situ Detection of the Diterpenoids with a Fluorescence Probe. The coumarin derived azide **51** is a fluorescence probe,[41] as it reacts with thiol to form fluorescent aminocoumarin **52**, enabling simple and sensitive quantification of hydrogen sulfide (Scheme S1 in the Supporting Information). By modifying this method, we found that it is also valid for the detection of intracellular thiol-based ingredients. As illustrated above, the *ent*-kaurane diterpenoids exert their biofunctions by interacting with intracellular thiols. The unreacted thiols can be detected by **51**. On the basis of this mechanism, the intracellular distribution of the diterpenoid can be monitored by observing the fluorescence using the probe. Here, with PC3 cells and the sulfhydryl group scavenger *N*-ethylmaleimide (NEM)[42−44] as a control, the performance of **46** was investigated by confocal microscopy.

As anticipated, incubation of PC3 cells with **51** resulted in a robust intracellular fluorescence signal, while preincubation with NEM reduced the level of fluorescence markedly (Figure 5A). With similar results, the level of fluorescence after preincubation of **46** decreased in a concentration- and time-dependent manner (Figure 5A,B). The intracellular fluorescence intensity, the statistical result by confocal fluorescence image analysis (Figure 5A,B), in turn demonstrated the potency of the cytotoxic activity. As shown in Table 1, **46** exhibited good cytotoxicity toward all of the tested cell lines. Its nonselective characteristic can be partly explained by the probe

DOI: 10.1021/acs.jmedchem.5b00208
J. Med. Chem. XXXX, XXX, XXX−XXX

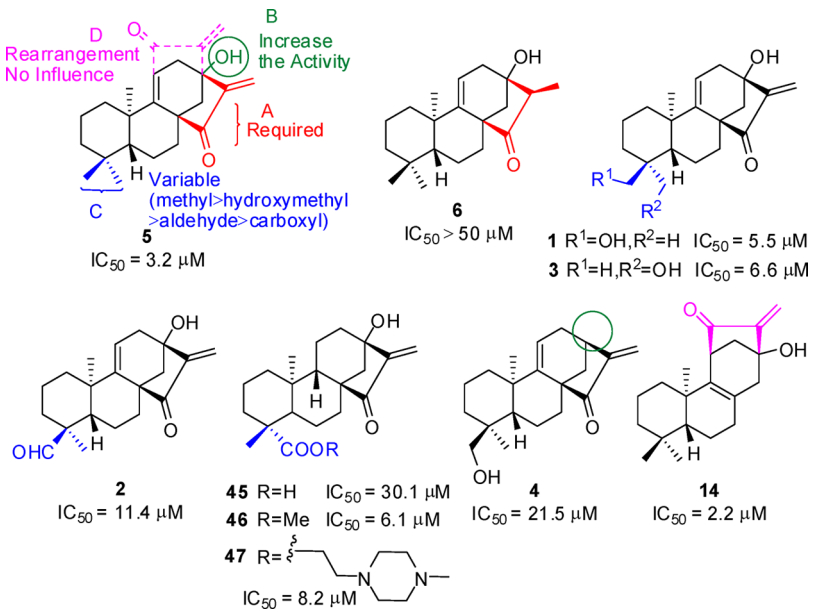

Figure 2. SAR summary of requirements for cytotoxicity. All of the IC_{50} values were measured against PC3 cells.

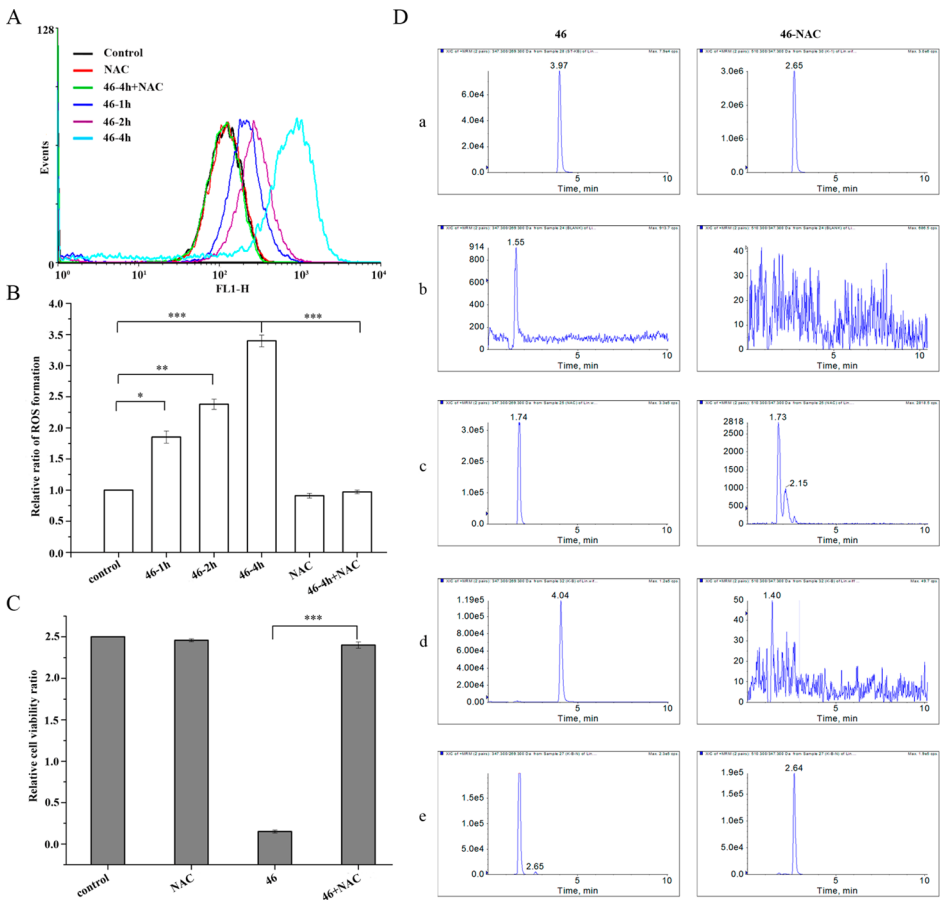

Figure 3. (A) Effect of **46** on the generation of ROS. PC3 cells exposed to 6 μM **46** for 4 h were collected, stained with DCFH-DA, and detected by flow cytometry. The antioxidant NAC (5.0 mM) was added for 1 h prior to **46**. (B) Statistical analysis of the relative ratio of ROS formation, **, $P < 0.01$ and ***, $P < 0.001$ compared with the control group or NAC-untreated group. (C) Effect of the antioxidant on **46**-induced cell death. PC3 cells were pretreated with 5 mM NAC for 1 h and then incubated with 6 μM **46** in the presence or absence of antioxidant for 24 h. Cell viability was then assessed by MTT assay. Data are shown as mean ± SD. ***, $P < 0.001$. (D) Detection of compounds **46** and **46−NAC** by HPLC−MS/MS: (a) standard substances; (b) cell culture medium; (c) cell culture medium with 5 mM NAC; (d) cell culture medium with 10 μM **46**; (e) cell culture medium with 5 mM NAC and 10 μM **46**.

DOI: 10.1021/acs.jmedchem.5b00208
J. Med. Chem. XXXX, XXX, XXX−XXX

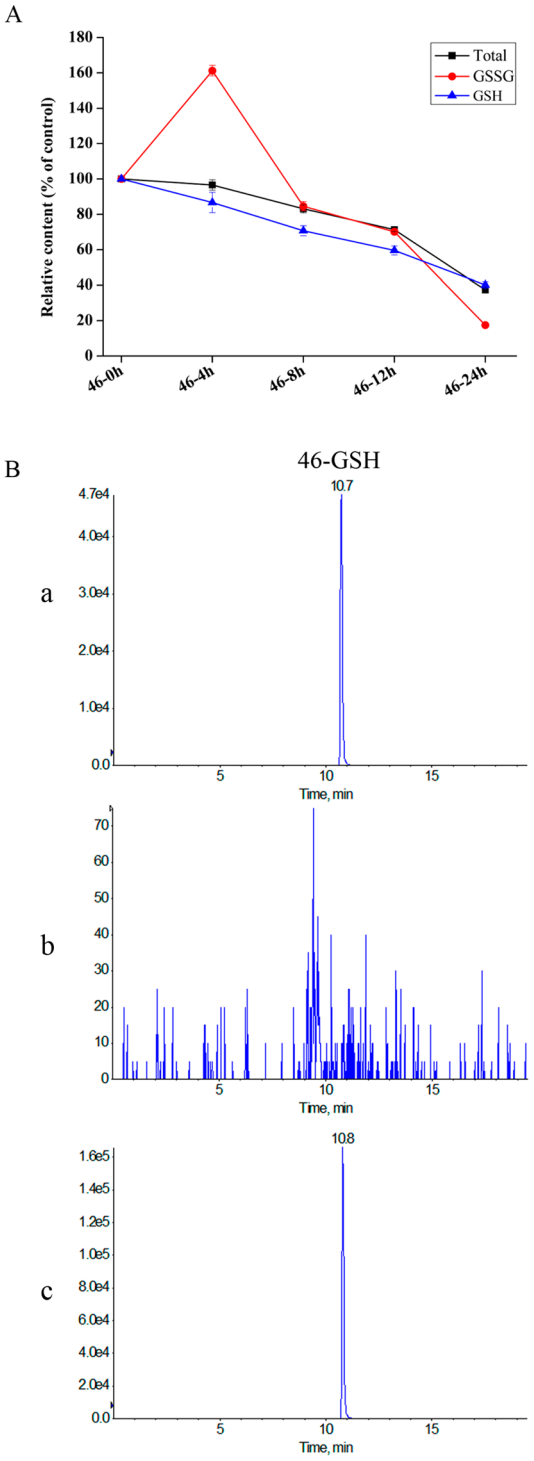

Figure 4. (A) Effect of **46** on the cellular GSH and GSSG levels. PC3 cells were exposed to 6 μM **46** for the indicated times. The results are presented as relative content of the treated cells compared with the control group. (B) Detection of **46−GSH** by HPLC−MS/MS: (a) standard substances; (b) control group; (c) cells treated with 6 μM **46** for 8 h.

staining results. In Figure 5A, compared with that of the control cells, the fluorescence of the drug-treated cells decreased homogeneously, suggesting the poor selectivity distribution. PC3 cells treated with different compounds at the same concentration, followed by incubation with **51**, were examined by confocal microscopy. As shown in Figure 5C, the fluorescence intensities were inversely proportional to the cytotoxicities of the compounds, suggesting that **51** can be applied as a probe to indicate the potency of these diterpenoids to kill the cancer cells.

The distribution behavior of a drug within a cell is an important variable in both activity and differential selectivity. Altered intracellular distribution of a drug is a way to improve drug selectivity.[45] From stevioside as a starting material, compound **47** was synthesized by introducing an *N*-methylpiperazine group. Again, by means of the above-established in situ detection method, the lysosomotropic ability and cytotoxic selectivity of **47** were tested. It is known that the lysosomes in cancer cells are more numerous and larger and that they have greater cathepsin activity than those in normal cells, and the release of cathepsins into the cytosol may result in apoptosis or necrosis.[46−48] A cytotoxicity test found that **47** showed higher activity toward PC3 cells (IC_{50} = 8.2 μM) while showing lower toxicity toward normal RWPE1 cells (IC_{50} = 29.3 μM), with improved selectivity (SI = 3.6). We also observed that lysosomes swelled or fused after treatment with **47** (Figure 5D). In situ detection with **51** still found a high value of the fluorescence intensity within the cells, indicating that there were more free thiols in the cytosol (Figure 5E). Meanwhile, the lower fluorescence in organelles suggests a high accumulation of **47**. The altered subcellular distribution of **47** led to cell death through the lysosome pathway by cathepsin B release, as shown in Figure 5F.

CONCLUSION

We have constructed a small library of *ent*-kaurane diterpenoids by isolation of natural products from liverworts and semisynthesis. Cytotoxicity screening showed that having an *exo*-methylene cyclopentanone moiety in these *ent*-kauranes is vital to their biological activity. The presence of a hydroxyl group on the C ring increased the activity, while the methyl oxidation at C-4 decreased the toxicity. Investigation of the mechanism revealed that these compounds kill the cancer cells through ROS-mediated apoptosis by the Michael reaction with the thiol-based proteins and depletion of intracellular GSH. A coumarin-based probe has been shown to be useful for detecting the cellular distribution of the diterpenoids by its reaction with free thiols. An alkaline derivative showed greatly improved selectivity to kill cancer cells as a result of its lysomotropic property. This provides a clue to develop this type of active diterpenoid into druggable candidates.

EXPERIMENTAL SECTION

General Materials and Methods. Melting points were determined on an X-6 melting point apparatus (Beijing TECH Instrument Co. Ltd.) and are uncorrected. Optical rotations were measured on a PerkinElmer 241 MC polarimeter. UV spectra were obtained with an Agilent 8453E UV−vis spectroscopy system. Electronic circular dichroism (CD) spectra were obtained on a Chirascan spectropolarimeter. IR spectra were recorded on a Nicolet iN 10 Micro FTIR spectrometer. NMR spectra were obtained using a Bruker Avance DRX-600 spectrometer operating at 600 (^{1}H) or 150 (^{13}C) MHz with tetramethylsilane as an internal standard. HR-ESI-MS was carried out on an LTQ Orbitrap XL instrument. HPLC was performed on an Agilent 1200 system equipped with a G1311A isopump, a G1322A degasser, and a G1315D DAD detector using a ZORBAX SB-C_{18} column (9.4 mm × 250 mm, 5 μm). All of the solvents used were of analytical grade. MCI gel (CHP20P, 75−150 μm, Mitsubishi Chemical Industries Ltd.), C_{18} reversed-phase silica gel (150−200 mesh, Merck), and Sephadex LH-20 (25−100 μm;

DOI: 10.1021/acs.jmedchem.5b00208
J. Med. Chem. XXXX, XXX, XXX−XXX

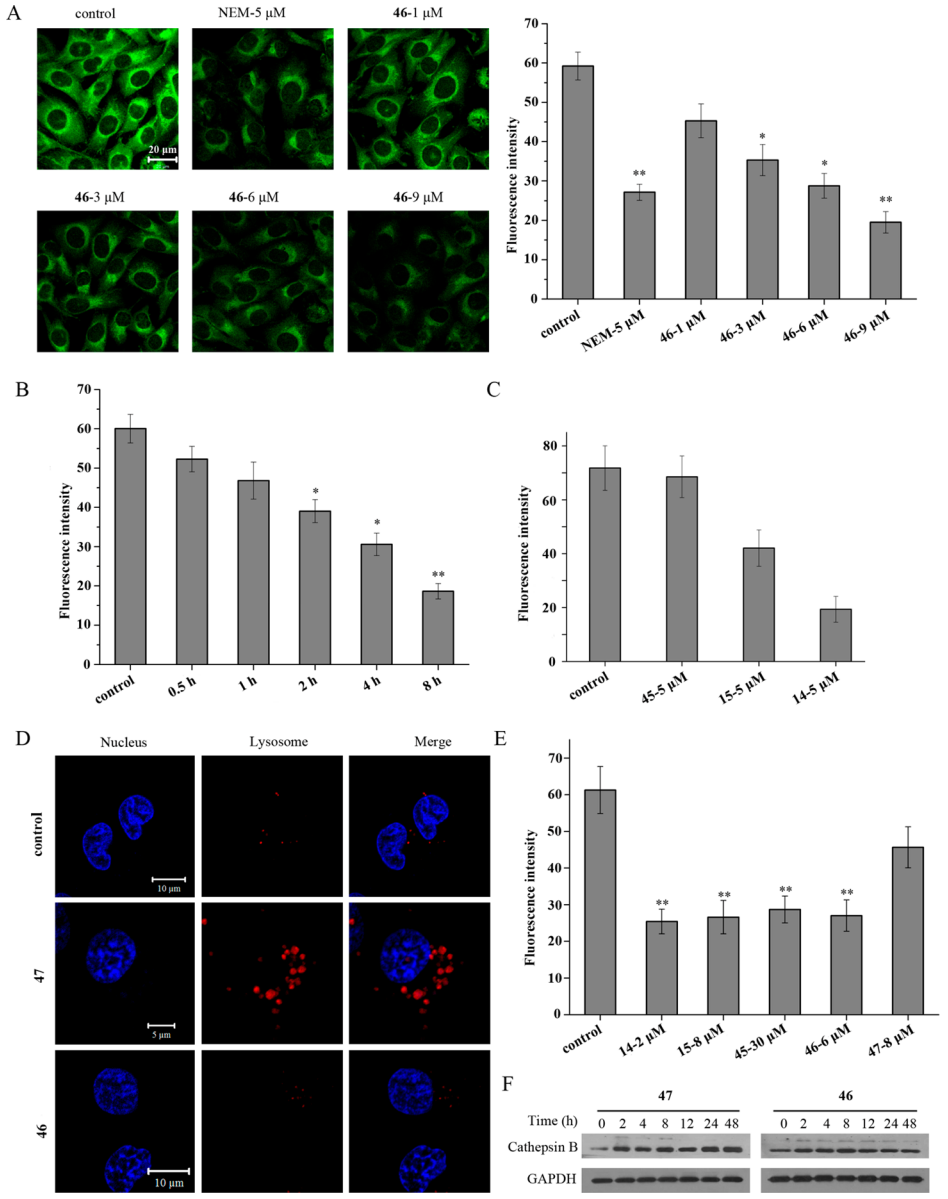

Figure 5. (A) Response of **51** with NEM and increasing concentrations of **46**. PC3 cells exposed to 5 μM NEM and different concentrations of **46** for 4 h were incubated with 30 μM **51** for 1 h in the dark and then examined by confocal microscopy (magnification 63× oil). The fluorescence intensities of different cell groups were quantitatively analyzed by confocal microscopy. (B) Quantitative analysis of the fluorescence intensities of different cell groups incubated with 30 μM **51** after treatment with **46** (6 μM) for different times. (C) Quantitative analysis of the fluorescence intensities of different cell groups incubated with 30 μM **51** after treatment with 5 μM **14**, **15**, and **45** for 4 h as measured by confocal microscopy. (D) PC3 cells exposed to **46** (6 μM) and **47** (8 μM) for 2 h were stained with LysoTracker Red and Hoechst 33342 and then measured by confocal microscopy. (E) Quantitative analysis of the fluorescence intensities of different cell groups incubated with 30 μM **51** after exposure to different compounds at the indicated concentrations for 4 h. All values are expressed as mean ± SD. *, $P < 0.05$ and **, $P < 0.01$. (F) Western blotting analysis of cathepsin B. PC3 cells were treated with **47** (8 μM) and **46** (6 μM) for the indicated times. GAPDH served as the loading control.

Pharmacia Biotek, Denmark) were used for column chromatography (CC). Precoated silica gel GF_{254} plates (Qingdao Haiyang Chemical Co., Ltd.) were used for thin-layer chromatography. Spots were visualized with UV light or by spraying with H_2SO_4/EtOH (1:9 v/v) followed by heating. The purities of all biologically evaluated compounds were established as ≥95% by HPLC analysis using two different gradients with UV detection (210, 254, and 280 nm).

Plant Material. The liverworts *J. fauriana* and *J. hyalina* were collected from Maoer Mountain, Guangxi Zhuang Autonomous Region, P. R. China, in April 2011 and authenticated by Prof. Yuan-Xin Xiong, College of Life Sciences, Guizhou University, P. R. China. Voucher specimens (no. 20110417-16 and no. 20110409-02) were deposited at the Department of Natural Products Chemistry, School of Pharmaceutical Sciences, Shandong University, P. R. China.

Extraction and Isolation. The air-dried powders of the plant material of *J. fauriana* (100.0 g) were extracted with 95% EtOH at room temperature (3 × 1.5 L, each for 1 week). Evaporation of the solvent in vacuo provided a dark residue (8.0 g), which was suspended in H_2O (150 mL) and partitioned with Et_2O (3 × 150 mL) successively. The Et_2O extract (5.1 g) was separated by MCI gel column chromatography (MeOH/H_2O, 3:7 to 9:1) to give six fractions (1–6). Fraction 2 (2.4 g) was chromatographed on a silica gel column [petroleum ether (60–90 °C)/acetone, 200:1 to 1:1] to give five subfractions (2.1–2.5). Fraction 2.2 (848.0 mg) was chromatographed on Sephadex LH-20 (MeOH) to obtain two fractions (2.2.1 and 2.2.2). Fraction 2.2.2 was separated by reversed-phase C18 HPLC (MeOH/H_2O, 7:3) and then purified by semipreparative HPLC (MeOH/H_2O, 80:20) to give **4** (3.4 mg, t_R

DOI: 10.1021/acs.jmedchem.5b00208
J. Med. Chem. XXXX, XXX, XXX–XXX

= 27.0 min), **21** (37.0 mg, t_R = 36.0 min), **22** (116.0 mg, t_R = 40.2 min), **23** (45.1 mg, t_R = 30.9 min), **16** (2.3 mg, t_R = 19.7 min), **a** (18.0 mg, t_R = 33.2 min), and **b** (12.2 mg, t_R = 28.8 min). **a** and **b** were further purified by semipreparative HPLC (acetonitrile/H_2O, 70:30) to give two pairs of compounds: **5** (10.0 mg, t_R = 31.3 min) and **6** (3.2 mg, t_R = 30.0 min) as well as **14** (9.0 mg, t_R = 26.7 min) and **18** (1.9 mg, t_R = 25.3 min). Fraction 2.3 (129.0 mg) was chromatographed on Sephadex LH-20 (MeOH) to obtain three fractions (2.3.1−2.3.3). Further separation of fraction 2.3.2 (89.0 mg) by reversed-phase C18 HPLC (MeOH/H_2O, 3:2) and then by semipreparative HPLC (MeOH/H_2O, 62:38) yielded **8** (5.3 mg, t_R = 20.9 min), **19** (6.5 mg, t_R = 16.5 min), and **c** (24.0 mg, t_R = 23.1 min), which was purified by semipreparative HPLC (acetonitrile/H_2O, 50:50) to give **2** (8.6 mg, t_R = 25.2 min) and **9** (12.0 mg, t_R = 23.1 min). Fraction 2.4 (651.0 mg) was chromatographed on Sephadex LH-20 (MeOH) and then separated by reversed-phase C18 HPLC (MeOH/H_2O, 7:3) to obtain three fractions (2.4.1−2.4.3). Fraction 2.4.1 was purified by semipreparative HPLC to give **20** (5.9 mg, t_R = 9.6 min), **d** (173.0 mg, t_R = 15.3 min), **e** (54.0 mg, t_R = 10.6 min), and **f** (18.0 mg, t_R = 12.4 min), which were further purified by semipreparative HPLC to afford **1** and **7** (72.0 mg/71.0 mg, 28.6 min/26.1 min; acetonitrile/H_2O, 40:60), **15** and **17** (3.5 mg/45.0 mg, 14.6 min/13.7 min; acetonitrile/H_2O, 45:55), and **3** and **10** (2.6 mg/13.0 mg, 14.9 min/13.7 min; acetonitrile/H_2O, 40:60), respectively. Fraction 2.5 (215.0 mg) was purified by Sephadex LH-20 column chromatography (MeOH) followed by semipreparative HPLC using MeOH/H_2O (68:32) as the mobile phase to yield **11** (1.2 mg, t_R = 21.0 min), **12** (3.2 mg, t_R = 24.5 min), and **13** (9.0 mg, t_R = 25.7 min). Fraction 3 (1.0 g) was also subjected to silica gel CC (petroleum ether/acetone, 200:1 to 5:1), which gave six fractions (3.1−3.6). Compound **24** (25.0 mg) was obtained from fraction 3.3 (92.0 mg) by Sephadex LH-20 column chromatography (CH_2Cl_2/MeOH, 1:1).

The air-dried powders of the plant material of *J. hyalina* (290.0 g) were extracted with 95% EtOH at room temperature (3 × 1.5 L, each for 1 week). Evaporation of the solvent in vacuo provided a dark residue (14.1 g), which was separated by MCI gel CC (MeOH/H_2O, 3:7 to 9:1) to yield three fractions (1−3). Fraction 2 (2.6 g) was chromatographed on a silica gel column [petroleum ether (60−90 °C)/acetone, 200:1 to 1:1] to give six subfractions (2.1−2.6). Fraction 2.2 (420.0 mg) was separated on Sephadex LH-20 (MeOH) to yield **24** (52.0 mg) and three new fractions (2.2.1−2.2.3). Fraction 2.2.2 (820.0 mg) was separated using reversed-phase C_{18} HPLC (MeOH/H_2O, 6:4 to 9:1) to yield five subfractions (2.2.2.1−2.2.2.5). Fraction 2.2.2.1 (18.0 mg) was purified by semipreparative HPLC (MeOH/H_2O, 78:22) to yield **33** (2.4 mg, t_R = 12.2 min), **35** (1.8 mg, t_R = 14.6 min), and **30** (3.2 mg, t_R = 17.9 min). Fraction 2.2.2.3 (23.5 mg) was separated using semipreparative HPLC (MeOH/H_2O, 80:20) to obtain **28** (15.0 mg, t_R = 15.0 min). Fraction 2.2.2.4 (27.0 mg) was purified by semipreparative HPLC (MeOH/H_2O, 84:76) to yield **42** (2.0 mg, t_R = 21.5 min), **34** (3.5 mg, t_R = 23.4 min), and **22** (7.0 mg, t_R = 28.4 min). Fraction 2.2.2.5 (25.2 mg) was separated using semipreparative HPLC (MeOH/H_2O, 90:10) to obtain **38** (11.0 mg, t_R = 24.5 min). Fraction 2.3 (346.0 mg) was chromatographed on Sephadex LH-20 (MeOH) and separated using reversed-phase C_{18} HPLC (MeOH/H_2O, 7:3 to 9:1) to yield five subfractions (2.3.1−2.3.5). Fraction 2.3.2 (75.4 mg) was separated by semipreparative HPLC (MeOH/H_2O, 72:28) to give **a** (41.0 mg, t_R = 24.0 min) and **b** (5.8 mg, t_R = 26.7 min), which were further purified by semipreparative HPLC (acetonitrile/H_2O, 50:50) to give **26** (1.6 mg, t_R = 7.3 min), **25** (34.0 mg, t_R = 11.4 min), and **27** (3.4 mg, t_R = 8.8 min). Fraction 2.3.3 (15.2 mg) was purified by semipreparative HPLC (acetonitrile/H_2O, 50:50) to give **39** (0.7 mg, t_R = 32.0 min). Fraction 2.3.4 (53.7 mg) was purified by the same method (acetonitrile/H_2O, 60:40) to give **29** (2.8 mg, t_R = 18.9 min), **37** (9.0 mg, t_R = 22.3 min), **32** (2.0 mg, t_R = 23.7 min), and **23** (23.0 mg, t_R = 26.9 min). Furthermore, separation of fraction 2.3.5 (13.0 mg) by semipreparative HPLC (MeOH/H_2O, 80:20) yielded **41** (1.9 mg, t_R = 25.6 min) and **36** (2.7 mg, t_R = 28.3 min). Fraction 3 (1.6 g) was chromatographed on a silica gel column [petroleum ether (60−90 °C)/acetone, 200:1 to 5:1] to give five subfractions (3.1−3.5). Fraction 3.2 (350.0 mg) was separated on Sephadex LH-20 (MeOH) and then separated using reversed-phase C_{18} HPLC (MeOH/H_2O, 6:4 to 9:1) to yield four subfractions (3.2.1−3.2.4). Fraction 3.2.3 (28.0 mg) was purified by semipreparative HPLC (acetonitrile/H_2O, 85:15) to yield **31** (2.4 mg, t_R = 20.4 min). Fraction 3.2.4 (33.4 mg) was purified by the same method (acetonitrile/H_2O, 95:5) to give **44** (9.0 mg, t_R = 31.6 min), **40** (8.0 mg, t_R = 33.1 min), and **43** (5.0 mg, t_R = 35.7 min).

13,18-Dihydroxy-ent-9(11),16-kauradien-15-one (**1**). Colorless needle crystals (MeOH); mp 164−166 °C; $[\alpha]_D^{25}$ = −21.90 (*c* 0.137, MeOH); UV (MeOH) λ_{max} (log ε) 350 (2.22), 227 (3.66), 208 (3.81) nm; CD (MeOH) λ_{max} ($\Delta\varepsilon$) 355 (+1.06), 278 (−0.36) nm; IR ν_{max} 3390, 2945, 1722, 1651 cm^{-1}; for ^1H and ^{13}C NMR data, see Tables S1 and S5; HR-ESI-MS (positive mode) *m*/*z* 334.2375 $[M + NH_4]^+$ (calcd for $C_{20}H_{32}O_3N$, 334.2377).

13-Hydroxy-ent-9(11),16-kauradien-18-al-15-one (**2**). Colorless oil; $[\alpha]_D^{25}$ = +18.52 (*c* 0.108, MeOH); UV (MeOH) λ_{max} (log ε) 206 (3.78) nm; CD (MeOH) λ_{max} ($\Delta\varepsilon$) 354 (+0.72), 311 (+0.60), 269 (−0.14) nm; IR ν_{max} 3425, 2931, 1718, 1647, 1456 cm^{-1}; for ^1H and ^{13}C NMR data, see Tables S1 and S5; HR-ESI-MS (positive mode) *m*/*z* 332.2220 $[M + NH_4]^+$ (calcd for $C_{20}H_{30}O_3N$, 332.2220).

13,19-Dihydroxy-ent-9(11),16-kauradien-15-one (**3**). Colorless needle crystals (MeOH); mp 169−170 °C; $[\alpha]_D^{25}$ = +112.5 (*c* 0.080, MeOH); UV (MeOH) λ_{max} (log ε) 206 (3.72) nm; CD (MeOH) λ_{max} ($\Delta\varepsilon$) 354 (+0.74), 278 (−0.22), 208 (+0.40) nm; IR ν_{max} 3328, 2956, 1708, 1641, 1462 cm^{-1}; for ^1H and ^{13}C NMR data, see Tables S1 and S5; HR-ESI-MS (positive mode) *m*/*z* 334.2393 $[M + NH_4]^+$ (calcd for $C_{20}H_{32}O_3N$, 334.2377).

18-Hydroxy-ent-9(11),16-kauradien-15-one (**4**). Colorless oil; $[\alpha]_D^{25}$ = −27.40 (*c* 0.073, MeOH); UV (MeOH) λ_{max} (log ε) 243 (3.38), 202 (3.61) nm; CD (MeOH) λ_{max} ($\Delta\varepsilon$) 321 (+0.35), 245 (−0.15) nm; IR ν_{max} 3417, 2926, 1712, 1647 cm^{-1}; for ^1H and ^{13}C NMR data, see Tables S1 and S5; HR-ESI-MS (positive mode) *m*/*z* 301.2161 $[M + H]^+$ (calcd for $C_{20}H_{29}O_2$, 301.2162).

13-Hydroxy-ent-9(11),16-kauradien-15-one (**5**). Colorless needle crystals (MeOH); mp 141−143 °C; $[\alpha]_D^{25}$ = −86.54 (*c* 0.104, MeOH); UV (MeOH) λ_{max} (log ε) 205 (3.77) nm; CD (MeOH) λ_{max} ($\Delta\varepsilon$) 221 (+0.61) nm; IR ν_{max} 3376, 2937, 1709, 1644 cm^{-1}; for ^1H and ^{13}C NMR data, see Tables S1 and S5; HR-ESI-MS (positive mode) *m*/*z* 301.2159 $[M + H]^+$ (calcd for $C_{20}H_{29}O_2$, 301.2162).

(16R)-13-Hydroxy-ent-9(11)-kauren-15-one (**6**). Colorless needle crystals (MeOH); mp 148−150 °C; $[\alpha]_D^{25}$ = +83.33 (*c* 0.144, MeOH); UV (MeOH) λ_{max} (log ε) 230 (3.08), 264 (1.96) nm; CD (MeOH) λ_{max} ($\Delta\varepsilon$) 303 (+3.81), 237 (−0.89) nm; IR ν_{max} 3364, 2927, 1733, 1456 cm^{-1}; for ^1H and ^{13}C NMR data, see Tables S1 and S5; HR-ESI-MS (positive mode) *m*/*z* 303.2320 $[M + H]^+$ (calcd for $C_{20}H_{31}O_2$, 303.2319).

(16R)-13,18-Dihydroxy-ent-9(11)-kauren-15-one (**7**). Colorless needle crystals (MeOH); mp 172−174 °C; $[\alpha]_D^{25}$ = +25.21 (*c* 0.119, MeOH); UV (MeOH) λ_{max} (log ε) 300 (2.32), 201 (3.61) nm; CD (MeOH) λ_{max} ($\Delta\varepsilon$) 303 (+3.57), 234 (−1.16), 213 (+0.42) nm; IR ν_{max} 3408, 2949, 1731, 1460 cm^{-1}; for ^1H and ^{13}C NMR data, see Tables S1 and S5; HR-ESI-MS (positive mode) *m*/*z* 336.2532 $[M + NH_4]^+$ (calcd for $C_{20}H_{34}O_3N$, 336.2533).

(16S)-13,18-Dihydroxy-ent-9(11)-kauren-15-one (**8**). Colorless needle crystals (MeOH); mp 182−184 °C; $[\alpha]_D^{25}$ = +111.11 (*c* 0.081, MeOH); UV (MeOH) λ_{max} (log ε) 300 (2.16), 224 (3.04), 201 (3.52) nm; CD (MeOH) λ_{max} ($\Delta\varepsilon$) 306 (+3.08), 238 (−0.41), 210 (+0.56) nm; IR ν_{max} 3417, 2931, 1733, 1459 cm^{-1}; for ^1H and ^{13}C NMR data, see Tables S1 and S5; HR-ESI-MS (positive mode) *m*/*z* 336.2533 $[M + NH_4]^+$ (calcd for $C_{20}H_{34}O_3N$, 336.2533).

(16R)-13-Hydroxy-ent-9(11)-kauren-18-al-15-one (**9**). Colorless oil; $[\alpha]_D^{25}$ = +47.06 (*c* 0.085, MeOH); UV (MeOH) λ_{max} (log ε) 279 (2.37), 204 (3.55) nm; CD (MeOH) λ_{max} ($\Delta\varepsilon$) 304 (+2.48), 235 (−0.68), 210 (+0.58) nm; IR ν_{max} 3418, 2937, 1726, 1456 cm^{-1}; for ^1H and ^{13}C NMR data, see Tables S2 and S5; HR-ESI-MS (positive mode) *m*/*z* 334.2372 $[M + NH_4]^+$ (calcd for $C_{20}H_{32}O_3N$, 334.2377).

(16R)-13,19-Dihydroxy-ent-9(11)-kauren-15-one (**10**). Colorless needle crystals (MeOH); mp 164−166 °C; $[\alpha]_D^{25}$ = +195.88 (*c* 0.097, MeOH); UV (MeOH) λ_{max} (log ε) 203 (3.42) nm; CD (MeOH) λ_{max} ($\Delta\varepsilon$) 303 (+3.41), 233 (−1.17), 212 (+0.68) nm; IR

DOI: 10.1021/acs.jmedchem.5b00208
J. Med. Chem. XXXX, XXX, XXX−XXX

ν_{max} 3389, 2956, 1722, 1661, 1461 cm^{-1}; for ^1H and ^{13}C NMR data, see Tables S2 and S5; HR-ESI-MS (positive mode) m/z 336.2533 $[M + NH_4]^+$ (calcd for $C_{20}H_{34}O_3N$, 336.2533).

(16R)-6α,13,18-Trihydroxy-ent-9(11)-kauren-15-one ***(11)***. White amorphous solid (MeOH); $[\alpha]_D^{25}$ = +100.00 (*c* 0.070, MeOH); UV (MeOH) λ_{max} (log ε) 295 (2.29), 202 (3.60) nm; CD (MeOH) λ_{max} ($\Delta\varepsilon$) 304 (+3.81), 233 (−1.22), 209 (+1.00) nm; IR ν_{max} 3424, 2990, 1724, 1466 cm^{-1}; for ^1H and ^{13}C NMR data, see Tables S2 and S5; HR-ESI-MS (positive mode) m/z 352.2482 $[M + NH_4]^+$ (calcd for $C_{20}H_{34}O_4N$, 352.2482).

(16R)-3α,11β-Dihydroxy-ent-kauran-15-one ***(12)***. Colorless needle crystals (MeOH); mp 196−197 °C; $[\alpha]_D^{25}$ = −108.33 (*c* 0.120, MeOH); UV (MeOH) λ_{max} (log ε) 201 (3.32) nm; CD (MeOH) λ_{max} ($\Delta\varepsilon$) 288 (+0.29), 235 (−0.09) nm; IR ν_{max} 3457, 2934, 1724, 1464 cm^{-1}; for ^1H and ^{13}C NMR data, see Tables S2 and S5; HR-ESI-MS (positive mode) m/z 338.2692 $[M + NH_4]^+$ (calcd for $C_{20}H_{36}O_3N$, 338.2690).

(16S)-3α,11β-Dihydroxy-ent-kauran-15-one ***(13)***. Colorless needle crystals (MeOH); mp 209−210 °C; $[\alpha]_D^{25}$ = −62.50 (*c* 0.080, MeOH); UV (MeOH) λ_{max} (log ε) 305 (2.51), 203 (2.95) nm; CD (MeOH) λ_{max} ($\Delta\varepsilon$) 330 (−0.05), 249 (+0.08) nm; IR ν_{max} 3425, 2931, 1725, 1444 cm^{-1}; for ^1H and ^{13}C NMR data, see Tables S2 and S5; HR-ESI-MS (positive mode) m/z 338.2689 $[M + NH_4]^+$ (calcd for $C_{20}H_{36}O_3N$, 338.2690).

13-Hydroxyjungermannenone B ***(14)***. Colorless needle crystals (MeOH); mp 171−173 °C; $[\alpha]_D^{25}$ = −267.44 (*c* 0.086, MeOH); UV (MeOH) λ_{max} (log ε) 350 (2.51), 269 (2.97), 207 (3.88) nm; CD (MeOH) λ_{max} ($\Delta\varepsilon$) 357 (−1.47), 281 (+0.66), 245 (−0.29) nm; IR ν_{max} 3478, 2926, 1717, 1651, 1473 cm^{-1}; for ^1H and ^{13}C NMR data, see Tables S2 and S5; HR-ESI-MS (positive mode) m/z 301.2149 $[M + H]^+$ (calcd for $C_{20}H_{29}O_2$, 301.2162).

13,18-Dihydroxyjungermannenone B ***(15)***. Colorless needle crystals (MeOH); mp 183−185 °C; $[\alpha]_D^{25}$ = −110.00 (*c* 0.100, MeOH); UV (MeOH) λ_{max} (log ε) 350 (2.54), 205 (3.89) nm; CD (MeOH) λ_{max} ($\Delta\varepsilon$) 357 (−1.27), 282 (+0.59), 247 (−0.20) nm; IR ν_{max} 3416, 2931, 1720, 1649, 1436 cm^{-1}; for ^1H and ^{13}C NMR data, see Tables S2 and S5; HR-ESI-MS (positive mode) m/z 334.2376 $[M + NH_4]^+$ (calcd for $C_{20}H_{32}O_3N$, 334.2377).

18-Hydroxyjungermannenone B ***(16)***. Colorless oil; $[\alpha]_D^{25}$ = −150.00 (*c* 0.080, MeOH); UV (MeOH) λ_{max} (log ε) 227 (3.34), 207 (3.46) nm; CD (MeOH) λ_{max} ($\Delta\varepsilon$) 319 (−0.75), 268 (+0.25), 206 (−0.38) nm; IR ν_{max} 3478, 2950, 1718, 1656, 1435 cm^{-1}; for ^1H and ^{13}C NMR data, see Tables S2 and S5; HR-ESI-MS (positive mode) m/z 301.2167 $[M + H]^+$ (calcd for $C_{20}H_{29}O_2$, 301.2162).

16α,17-Dihydro-13,18-dihydroxyjungermannenone B ***(17)***. Colorless needle crystals (MeOH); mp 202−204 °C; $[\alpha]_D^{25}$ = −68.63 (*c* 0.102, MeOH); UV (MeOH) λ_{max} (log ε) 300 (2.42), 229 (3.07), 203 (3.58) nm; CD (MeOH) λ_{max} ($\Delta\varepsilon$) 300 (−3.75), 240 (+1.41), 206 (−0.20) nm; IR ν_{max} 3481, 2938, 1720, 1681, 1390 cm^{-1}; for ^1H and ^{13}C NMR data, see Tables S2 and S6; HR-ESI-MS (positive mode) m/z 336.2535 $[M + NH_4]^+$ (calcd for $C_{20}H_{34}O_3N$, 336.2533).

16α,17-Dihydro-13-hydroxyjungermannenone B ***(18)***. White amorphous solid (MeOH); $[\alpha]_D^{25}$ = −100.92 (*c* 0.109, MeOH); UV (MeOH) λ_{max} (log ε) 300 (2.40), 229 (3.08), 204 (3.52) nm; CD (MeOH) λ_{max} ($\Delta\varepsilon$) 300 (−3.09), 236 (+1.15), 211 (−0.33) nm; IR ν_{max} 3472, 2935, 1724, 1457 cm^{-1}; for ^1H and ^{13}C NMR data, see Tables S3 and S6; HR-ESI-MS (positive mode) m/z 320.2578 $[M + NH_4]^+$ (calcd for $C_{20}H_{34}O_2N$, 320.2584).

18-Formyl-16α,17-dihydro-13-hydroxyjungermannenone B ***(19)***. Colorless oil; $[\alpha]_D^{25}$ = −155.84 (*c* 0.077, MeOH); UV (MeOH) λ_{max} (log ε) 300 (2.57), 244 (3.26), 205 (3.50) nm; CD (MeOH) λ_{max} ($\Delta\varepsilon$) 306 (−1.74), 257 (+0.34), 238 (+0.29), 211 (−0.25) nm; IR ν_{max} 3416, 2938, 1729, 1664, 1454 cm^{-1}; for ^1H and ^{13}C NMR data, see Tables S3 and S6; HR-ESI-MS (positive mode) m/z 334.2374 $[M + NH_4]^+$ (calcd for $C_{20}H_{32}O_3N$, 334.2377).

16α,17-Dihydro-13,19-dihydroxyjungermannenone B ***(20)***. Colorless needle crystals (MeOH); mp 198−199 °C; $[\alpha]_D^{25}$ = −134.62 (*c* 0.052, MeOH); UV (MeOH) λ_{max} (log ε) 300 (2.63), 202 (3.77) nm; CD (MeOH) λ_{max} ($\Delta\varepsilon$) 300 (−3.94), 235 (+1.81), 209 (−0.69) nm; IR ν_{max} 3428, 2932, 1721, 1453 cm^{-1}; for ^1H and ^{13}C NMR data, see Tables S3 and S6; HR-ESI-MS (positive mode) m/z 336.2548 $[M + NH_4]^+$ (calcd for $C_{20}H_{34}O_3N$, 336.2533).

6α,15β-Dihydroxy-ent-16-kauren-11-one ***(25)***. Colorless needle crystals (MeOH); mp 167−169 °C; $[\alpha]_D^{25}$ = +207.92 (*c* 0.101, MeOH); UV (MeOH) λ_{max} (log ε) 208 (2.79) nm; CD (MeOH) λ_{max} ($\Delta\varepsilon$) 310 (+0.78), 221 (+1.05) nm; IR ν_{max} 3522, 2919, 1687, 1659, 1415 cm^{-1}; for ^1H and ^{13}C NMR data, see Tables S3 and S6; HR-ESI-MS (positive mode) m/z 336.2535 $[M + NH_4]^+$ (calcd for $C_{20}H_{34}O_3N$, 336.2533).

6α,7α,15β-Trihydroxy-ent-16-kauren-11-one ***(26)***. Colorless needle crystals (MeOH); mp 173−175 °C; $[\alpha]_D^{25}$ = +175.93 (*c* 0.108, MeOH); UV (MeOH) λ_{max} (log ε) 204 (2.75) nm; CD (MeOH) λ_{max} ($\Delta\varepsilon$) 310 (+0.40), 222 (+1.18) nm; IR ν_{max} 3415, 2948, 1688, 1408 cm^{-1}; for ^1H and ^{13}C NMR data, see Tables S3 and S6; HR-ESI-MS (positive mode) m/z 352.2483 $[M + NH_4]^+$ (calcd for $C_{20}H_{34}O_4N$, 352.2482).

7α,15β-Dihydroxy-ent-16-kauren-11-one ***(27)***. Colorless needle crystals (MeOH); mp 209−211 °C; $[\alpha]_D^{25}$ = +183.67 (*c* 0.098, MeOH); UV (MeOH) λ_{max} (log ε) 305 (1.55), 206 (2.79) nm; CD (MeOH) λ_{max} ($\Delta\varepsilon$) 310 (+0.61), 222 (+1.42) nm; IR ν_{max} 3518, 2950, 1701, 1058 cm^{-1}; for ^1H and ^{13}C NMR data, see Tables S3 and S6; HR-ESI-MS (positive mode) m/z 336.2533 $[M + NH_4]^+$ (calcd for $C_{20}H_{34}O_3N$, 336.2533).

15β-Hydroxy-ent-16-kauren-11-one ***(28)***. Colorless needle crystals (MeOH); mp 140−142 °C; $[\alpha]_D^{25}$ = +186.29 (*c* 0.102, MeOH); UV (MeOH) λ_{max} (log ε) 306 (1.58), 207 (2.82) nm; CD (MeOH) λ_{max} ($\Delta\varepsilon$) 311 (+0.96), 222 (+1.61) nm; IR ν_{max} 3389, 2921, 1692, 1655 cm^{-1}; for ^1H and ^{13}C NMR data, see Tables S3 and S6; HR-ESI-MS (positive mode) m/z 320.2582 $[M + NH_4]^+$ (calcd for $C_{20}H_{34}O_2N$, 320.2584).

1α,15β-Dihydroxy-ent-16-kaurene ***(29)***. Colorless needle crystals (MeOH); mp 182−185 °C; $[\alpha]_D^{25}$ = −86.54 (*c* 0.104, MeOH); UV (MeOH) λ_{max} (log ε) 208 (2.77) nm; CD (MeOH) λ_{max} ($\Delta\varepsilon$) 355 (+0.76), 276 (−0.44), 221 (+0.61) nm; IR ν_{max} 3376, 2937, 1709, 1644 cm^{-1}; for ^1H and ^{13}C NMR data, see Tables S4 and S6; HR-ESI-MS (positive mode) m/z 322.2739 $[M + NH_4]^+$ (calcd for $C_{20}H_{36}O_2N$, 322.2741).

1α,15α-Dihydroxy-ent-16-kaurene ***(30)***. Colorless needle crystals (MeOH); mp 166−168 °C; $[\alpha]_D^{25}$ = +218.18 (*c* 0.055, MeOH); UV (MeOH) λ_{max} (log ε) 205 (2.96) nm; CD (MeOH) λ_{max} ($\Delta\varepsilon$) 311 (+0.11), 211 (−1.05) nm; IR ν_{max} 3328, 2927, 1445, 1057 cm^{-1}; for ^1H and ^{13}C NMR data, see Tables S4 and S6; HR-ESI-MS (positive mode) m/z 322.2740 $[M + NH_4]^+$ (calcd for $C_{20}H_{36}O_2N$, 322.2741).

9β,15β-Dihydroxy-ent-16-kaurene ***(31)***. Colorless needle crystals (MeOH); mp 165−166 °C; $[\alpha]_D^{25}$ = +100.00 (*c* 0.070, MeOH); UV (MeOH) λ_{max} (log ε) 209 (2.84) nm; CD (MeOH) λ_{max} ($\Delta\varepsilon$) 210 (+0.24) nm; IR ν_{max} 3409, 2929, 1713, 1459 cm^{-1}; for ^1H and ^{13}C NMR data, see Tables S4 and S6; HR-ESI-MS (positive mode) m/z 322.2743 $[M + NH_4]^+$ (calcd for $C_{20}H_{36}O_2N$, 322.2741).

11α,15β-Dihydroxy-ent-16-kaurene ***(32)***. Colorless needle crystals (MeOH); mp 179−181 °C; $[\alpha]_D^{25}$ = +127.91 (*c* 0.086, MeOH); UV (MeOH) λ_{max} (log ε) 209 (2.83) nm; CD (MeOH) λ_{max} ($\Delta\varepsilon$) 308 (−0.07), 213 (+0.53) nm; IR ν_{max} 3365, 2929, 1449, 1052 cm^{-1}; for ^1H and ^{13}C NMR data, see Tables S4 and S6; HR-ESI-MS (positive mode) m/z 322.2739 $[M + NH_4]^+$ (calcd for $C_{20}H_{36}O_2N$, 322.2741).

1α,7α-Dihydroxy-ent-16-kaurene ***(33)***. Colorless needle crystals (MeOH); mp 174−176 °C; $[\alpha]_D^{25}$ = +56.19 (*c* 0.133, MeOH); UV (MeOH) λ_{max} (log ε) 206 (2.77) nm; CD (MeOH) λ_{max} ($\Delta\varepsilon$) 219 (+1.02) nm; IR ν_{max} 3385, 2928, 1457, 1028 cm^{-1}; for ^1H and ^{13}C NMR data, see Tables S4 and S6; HR-ESI-MS (positive mode) m/z 322.2738 $[M + NH_4]^+$ (calcd for $C_{20}H_{36}O_2N$, 322.2741).

7α-Acetoxy-1α-hydroxy-ent-16-kaurene ***(34)***. Colorless needle crystals (MeOH); mp 172−174 °C; $[\alpha]_D^{25}$ = +38.46 (*c* 0.130, MeOH); UV (MeOH) λ_{max} (log ε) 209 (2.73) nm; CD (MeOH) λ_{max} ($\Delta\varepsilon$) 218 (+0.28) nm; IR ν_{max} 3445, 2925, 1728, 1704, 1242 cm^{-1}; for ^1H and ^{13}C NMR data, see Tables S4 and S6; HR-ESI-MS (positive mode) m/z 364.2843 $[M + NH_4]^+$ (calcd for $C_{22}H_{38}O_3N$, 364.2846).

1α,7α-Dihydroxy-ent-15-kaurene ***(35)***. Colorless needle crystals (MeOH); mp 159−161 °C; $[\alpha]_D^{25}$ = +66.17 (*c* 0.136, MeOH); UV (MeOH) λ_{max} (log ε) 209 (2.70) nm; CD (MeOH) λ_{max} ($\Delta\varepsilon$) 218

DOI: 10.1021/acs.jmedchem.5b00208
J. Med. Chem. XXXX, XXX, XXX−XXX

(+0.31) nm; IR ν_{max} 3371, 2928, 1461, 1018 cm^{-1}; for ^1H and ^{13}C NMR data, see Tables S4 and S6; HR-ESI-MS (positive mode) m/z 322.2740 $[M + NH_4]^+$ (calcd for $C_{20}H_{36}O_2N$, 322.2741).

*15β-Acetoxy-ent-kaur-16-en-18-oic Acid (**36**).* Colorless needle crystals (MeOH); mp 186−188 °C; $[\alpha]_D^{25}$ = +11.36 (*c* 0.088, MeOH); UV (MeOH) λ_{max} (log ε) 206 (2.91) nm; CD (MeOH) λ_{max} ($\Delta\varepsilon$) 221 (−0.15) nm; IR ν_{max} 3362, 2930, 1730, 1708 cm^{-1}; for ^1H and ^{13}C NMR data, see Tables S4 and S6; HR-ESI-MS (positive mode) m/z 378.2639 $[M + NH_4]^+$ (calcd for $C_{22}H_{38}O_4N$, 378.2639).

*ent-13-Hydroxy-15-kaurene-19-acid (**45**).* To a solution of stevioside (2.0 g, 2.48 mmol) in 150 mL of deionized water was added $NaIO_4$ (3.0 g, 14.02 mmol). The mixture was stirred for 16 h with hydrogen at room temperature and then at 0 °C. Then KOH (15.0 g, 267.86 mmol) was added slowly to the resulting solution, which was subsequently refluxed for 1 h. The resulting solution was cooled, acidified with acetate to a pH of 3−4, and extracted with ethyl ether (3 × 100 mL). The combined extracts were washed with distilled water and brine, dried over $MgSO_4$, and evaporated under vacuum to obtain the crude product, which was then purified by flash chromatography to give 500.0 mg of steviol. To a solution of steviol (400.0 mg, 1.26 mmol) in 12 mL of THF were added SeO_2 (100.0 mg, 0.90 mmol) and *t*-BuOOH (680 μL, 7.08 mmol) in 12 mL of THF. After 20 of stirring at room temperature, saturated brine with a slight amount of $NaHSO_3$ was added to the resulting solution, which was then extracted twice with EtOAc. The combined extracts were washed with brine, dried over $MgSO_4$, and evaporated under vacuum to obtain the crude product, which was then purified by flash chromatography to give compound **48** (210.0 mg, powder, 51%). Compound **48** (70.0 mg, 0.21 mmol) and PDC (73.0 mg, 0.19 mmol) were reacted in 1.5 mL of DMF for 12 h at room temperature. Then saturated brine was poured into the resulting solution, which was extracted with EtOAc. The combined extracts were washed with brine, dried over $MgSO_4$, and evaporated under vacuum to obtain the crude product, which was then purified by flash chromatography to give compound **45** (50.0 mg, 72%). Colorless needles ($CHCl_3$); HR-ESI-MS (positive mode) m/z 350.2327 $[M + NH_4]^+$ (calcd for $C_{20}H_{32}O_4N$, 350.2326); ^1H NMR ($CDCl_3$, 600 MHz) δ_H 6.05 (1H, s, H-17a), 5.44 (1H, s, H-17b), 1.27 (3H, s, H_3-18), 1.03 (3H, s, H_3-20); ^{13}C NMR ($CDCl_3$, 150 MHz) δ_C 39.6 (C-1), 18.7 (C-2), 37.5 (C-3), 43.5 (C-4), 55.9 (C-5), 20.0 (C-6), 32.7 (C-7), 55.1 (C-8), 50.2 (C-9), 40.2 (C-10), 20.7 (C-11), 39.1 (C-12), 77.1 (C-13), 44.8 (C-14), 208.3 (C-15), 151.1 (C-16), 115.1 (C-17), 28.7 (C-18), 182.6 (C-19), 15.4 (C-20).

*ent-13-Hydroxy-15-kaurene-19-acid Methyl Ester (**46**).* To a solution of compound **45** (30.0 mg, 0.09 mmol) in 2 mL of DMF were added anhydrous K_2CO_3 (32.0 mg, 0.23 mmol) and MeI (28.0 μL, 0.45 mmol). The mixture was stirred for 8 h at room temperature. Then 3 mL of water were added to the resulting solution, which was extracted with EtOAc (10 mL × 2). The combined extracts were washed with brine, dried over $MgSO_4$, and evaporated under vacuum to obtain the crude product, which was then purified by flash chromatography to give compound **46** (21.0 mg, 68%). Colorless needles ($CHCl_3$); HR-ESI-MS (positive mode) m/z 364.2482 $[M + NH_4]^+$ (calcd for $C_{21}H_{34}O_4N$, 364.2482); ^1H NMR ($CDCl_3$, 600 MHz) δ_H 6.04 (1H, s, H-17a), 5.43 (1H, s, H-17b), 3.66 (3H, s, $-OCH_3$), 1.20 (3H, s, H_3-18), 0.89 (3H, s, H_3-20). ^{13}C NMR ($CDCl_3$, 150 MHz) δ_C 39.8 (C-1), 18.8 (C-2), 37.8 (C-3), 43.7 (C-4), 56.0 (C-5), 20.0 (C-6), 32.8 (C-7), 55.1 (C-8), 50.2 (C-9), 40.0 (C-10), 20.7 (C-11), 39.1 (C-12), 77.0 (C-13), 44.7 (C-14), 208.5 (C-15), 151.4 (C-16), 115.4 (C-17), 28.7 (C-18), 177.8 (C-19), 15.3 (C-20), 51.3 ($-OCH_3$).

*ent-13-Hydroxy-15-kaurene-19-acid N-Methylpiperazine Ethyl Ester (**47**).* To a solution of compound **48** (100.0 mg, 0.30 mmol) in 5 mL of DMF were added 1,2-dibromoethane (0.24 mL, 2.78 mmol) and anhydrous K_2CO_3 (190.0 mg, 1.37 mmol). The mixture was stirred for 4 h at room temperature. Then 10 mL of water was added to the resulting solution, which was extracted with EtOAc (15 mL × 2). The combined extracts were washed with brine, dried over $MgSO_4$, and evaporated under vacuum to obtain compound **49** (120.0 mg), which was then dissolved in 10 mL of water and reacted with *N*-methylpiperazine (0.10 mL, 0.90 mmol) and anhydrous K_2CO_3 (110.0 g, 0.79 mmol) for 10 h under reflux. Then 10 mL of water was added to the resulting solution, which was extracted with EtOAc (15 mL × 2). The combined extracts were washed with brine, dried over $MgSO_4$, and evaporated under vacuum to obtain compound **50** (75.0 mg), which was then dissolved in 2 mL of DMF and reacted with PDC (75.0 mg, 0.20 mmol) for 12 h at room temperature. Then 10 mL of water was added to the resulting solution, which was extracted with EtOAc (15 mL × 2). The combined extracts were washed with brine, dried over $MgSO_4$, and evaporated under vacuum to obtain the crude product, which was then purified by flash chromatography to give compound **47** (40.0 mg, 29%). Colorless oil; HR-ESI-MS (positive mode) m/z 459.3216 $[M + H]^+$ (calcd for $C_{27}H_{43}O_4N_2$, 459.3217); ^1H NMR ($CDCl_3$, 600 MHz) δ_H 6.04 (1H, s, H-17a), 5.44 (1H, s, H-17b), 2.59 (3H, s, $-NCH_3$), 1.20 (3H, s, H_3-18), 0.93 (3H, s, H_3-20); ^{13}C NMR ($CDCl_3$, 150 MHz) δ_C 39.8 (C-1), 18.8 (C-2), 37.9 (C-3), 43.8 (C-4), 56.0 (C-5), 20.1 (C-6), 32.9 (C-7), 55.1 (C-8), 50.1 (C-9), 40.1 (C-10), 20.7 (C-11), 39.2 (C-12), 77.0 (C-13), 44.8 (C-14), 208.4 (C-15), 151.3 (C-16), 115.3 (C-17), 28.8 (C-18), 177.2 (C-19), 15.6 (C-20), 61.1 (C-1′), 56.1 (C-2′), 51.1 (C-3′, C-5′), 54.3 (C-4′, C-6′), 44.8 ($-NCH_3$).

X-ray Crystal Structure Analysis. A colorless crystal of **1** was obtained from MeOH. Intensity data were collected on a Bruker APEX DUO diffractometer equipped with an APEX II CCD using Cu Kα radiation. Cell refinement and data reduction were performed with Bruker SAINT. The structures were solved by direct methods using SHELXS-97.[49] Refinements were performed with SHELXL-97 using full-matrix least-squares with anisotropic displacement parameters for all of the non-hydrogen atoms. The H atoms were placed in calculated positions and refined using a riding model. Molecular graphics were computed with SHELXS-97. Crystallographic data for the structure of **1** (excluding structure factor tables) have been deposited with the Cambridge Crystallographic Data Centre as supplementary publication CCDC 1046802. Copies of the data can be obtained free of charge on application to the CCDC, 12 Union Road, Cambridge CB2 1EZ, U.K. [fax: Int. +44(0) (1223) 336 033; e-mail: deposit@ccdc.cam.ac.uk].

*Crystal Data for 13,18-Dihydroxy-ent-9(11),16-kauradien-15-one (**1**).* $C_{20}H_{28}O_3$, MW = 316.43, orthorhombic, a = 13.0132(11) Å, b = 21.6913(16) Å, c = 6.3473(6) Å, α = 90.00°, β = 90.00°, γ = 90.00°, V = 1791.7(3) $Å^3$, T = 293(2) K, space group $P2$, Z = 4, μ(Cu Kα) = 0.643 mm^{-1}, 3845 reflections measured, 2634 independent reflections (R_{int} = 0.0321). The final R_1 values were 0.0512 ($I > 2\sigma(I)$) and 0.0676 (all data). The final $wR(F^2)$ values were 0.1169 ($I > 2\sigma(I)$) and 0.1312 (all data). The goodness of fit on F^2 was 1.017, and the Flack parameter was −0.1(4).

Synthesis of Compound 46−NAC. To a solution of compound **46** (10.0 mg) in 1.5 mL of MeOH was added 5.0 mg of NAC in 0.5 mL of water. The pH of the mixture was adjusted to 9 with aqueous ammonia. Then the mixture was stirred for 0.5 h at room temperature to give the target compound. HR-ESI-MS (positive mode) m/z 510.2517 $[M + H]^+$ (calcd for $C_{26}H_{40}O_7NS$, 510.2520).

Synthesis of Compound 46−GSH. To a solution of compound **46** (10.0 mg) in 1.5 mL of MeOH was added 5.0 mg of GSH in 0.5 mL of water. The pH of the mixture was adjusted to 9 with aqueous ammonia. Then the mixture was stirred for 0.5 h at room temperature to give the target compound. HR-ESI-MS (positive mode) m/z 654.3039 $[M + H]^+$ (calcd for $C_{31}H_{48}O_{10}N_3S$, 654.3055).

HPLC−MS/MS Analysis. The HPLC−MS/MS system consisted of an Agilent 1260 series binary pump (Agilent Technologies, Palo Alto, CA, USA) and a Shiseido 5100 autosampler connected to an API 4000 mass spectrometer (Applied Biosystems Sciex, Ontario, Canada) using a turbospray ionization source (ESI). The instrument was interfaced to a computer running Applied Biosystems Analyst version 1.4.2 software.

Compounds were separated on a ZORBAX SB-C18 column (5 μm, 150 mm × 2.1 mm I.D., Agilent Science Inc., USA) through a 4 mm × 3 mm precolumn (Security Guard C_{18} cartridge, Phenomenex, Inc.) maintained at room temperature. The mobile phase consisted of acetonitrile−0.5% formic acid/water (70:30 v/v) (pH 2.5) and was set at a flow rate of 0.25 mL/min. The detector was operated at unit resolution in the positive multiple-reaction monitoring (+MRM)

DOI: 10.1021/acs.jmedchem.5b00208
J. Med. Chem. XXXX, XXX, XXX−XXX

mode using the transitions of the protonated molecular ions of **46** (*m*/*z* 347.3; *m*/*z* 269.2) and **46−NAC** (*m*/*z* 510.3; *m*/*z* 347.3). The optimized parameters were as follows: the curtain gas, gas1, and gas2 (nitrogen) pressures were 25, 50, and 40 psi, respectively; the dwell time was 200 ms; the source temperature was 500 °C; the ion spray voltage was 4800 V. The declustering potential and collision energy were 60 and 20 V for **46** and 50 and 25 V for **46−NAC**, respectively.

Compounds were separated on a ZORBAX SB-C18 column (5 μm, 150 mm × 2.1 mm I.D., Agilent Science Inc., USA) through a 4 mm × 3 mm precolumn (Security Guard C_{18} cartridge, Phenomenex, Inc.) maintained at room temperature. The mobile phase consisted of acetonitrile−0.5% formic acid/water (80:20 v/v) (pH 2.5) and was set at a flow rate of 0.30 mL/min. The detector was operated at unit resolution in the negative multiple-reaction monitoring (−MRM) mode using the transitions of the protonated molecular ions of **46−GSH** (652.3 *m*/*z*; 306.2 *m*/*z*). The optimized parameters were as follows: the curtain gas, gas1, and gas2 (nitrogen) pressures were 15, 30, and 50 psi, respectively; the dwell time was 200 ms; the source temperature was 500 °C; the ion spray voltage was −4200 V. The declustering potential and collision energy were −65 and −27 V, respectively, for**46−GSH**.

Cell Culture and Treatments. The human prostate carcinoma cell lines PC3, DU145, and LNCaP, the lung cancer cell line NCI-H1299, the breast carcinoma cell line MDA-MB231, the colon cancer cell line LOVO, the urinary bladder carcinoma cell line T24, and the myelogenous leukemia cell lines K562 and HL-60 were cultured in RPMI 1640 medium (Hyclone, Logan, UT) supplemented with 10% fetal bovine serum (FBS) (Hyclone), 100 units/mL penicillin, and 100 μg/mL streptomycin. The human astrocytoma cell lines A172 and SH-SY5Y and the osteosarcoma cell line Saos-2 were cultured in DMEM/HIGH GLUCOSE medium supplemented with 10% FBS, 5% mare serum (Hyclone), 100 units/mL penicillin, and 100 μg/mL streptomycin. The human ovarian cancer cell line SKOV3 was cultured in McCoy's 5A medium (Hyclone, Logan, UT) supplemented with 10% FBS, 100 units/mL penicillin, and 100 μg/mL streptomycin. The human prostate epithelial cell line RWPE-1 was maintained in Keratinocyte1 medium (K-SFM) supplemented with 50 mg/L bovine pituitary extract and 5 μg/L epidermal growth factor (Gibco, Grand Island, NY). The cells were maintained in 5% CO_2 at 37 °C until they reached approximately 50−70% confluence and were then treated with various concentrations of compounds. Dimethyl sulfoxide (DMSO) was used as the control vehicle.

Cell Proliferation Assay. An MTT [3-(4,5-dimethylthiazol-2-yl)-2,5-diphenyl-2*H*-tetrazolium bromide, Sigma, St. Louis, MO] assay was used to measure the proliferation of cells treated with different compounds in 96-well plates. After treatment with vehicle, the compounds alone, or cisplatin as a positive control for 24 h, the cells were incubated with 10 μL of MTT (5 mg/mL) for 4 h. The formazan product was then solubilized with 100 μL of DMSO. The absorbance was measured at 570 nm using a microplate reader (Bio-Rad, USA). The IC_{50} value was calculated based on percent cell viability using GraphPad Prism 5.0 (La Jolla, CA). All of the experiments were conducted at least three times. In some experiments, cells were exposed to 5 mM NAC (Sigma-Aldrich, USA) for 1 h prior to treatment with compound **46**. The cell proliferations in response to the compounds were analyzed using the MTT assay.

Microscopy. PC3 cells were seeded on 6 mm round glass coverslips and placed at the bottom of 24-well plates. After different treatments, cells on glass coverslips were fixed with cold methanol/acetone (1:1) for 5 min. After washing, cells were incubated with 30 μM probe **51** for 1 h at room temperature in the dark. Fluorescence images were captured using a confocal microscope (Carl Zeiss). The mean fluorescence intensity of cells was measured using ZEN 2010 software. Cells were defined using a free-form selection tool.

To measure the volume of lysosomes, PC3 cells in various stages after treatment were incubated at 37 °C for 30 min with 100 ng/mL LysoTracker (Molecular Probes) and 10 μg/mL Hoechst 33342 (Sigma-Aldrich). Cells were then washed with phosphate-buffered saline (PBS) for measurement of the fluorescence derived from the aggregated LysoTracker in acidic compartments using a confocal microscope.

ROS Measurement. Intracellular ROS accumulation was monitored using the fluorescent probe DCFH-DA. After treatment with **46** for the indicated times, PC3 cells were incubated with 10 μM DCFH-DA at 37 °C for 30 min. Cells were washed, collected, resuspended in PBS, and analyzed immediately using flow cytometry (Becton Dickinson, USA). In some experiments, cells were pretreated with 5 mM NAC for 1 h prior to exposure with **46** and analyzed for ROS generation.

GSH and GSSG Analyses. Cellular GSH and GSSG levels were measured by the method of Griffith.[50] PC3 cells exposed to 6 μM **46** for the indicated times were collected and resuspended in a protein removal agent to collect supernatant by centrifugation after repeated freezing and thawing. Total GSH and GSSG were measured after the addition of dithiobis(2-nitrobenzoic acid) (DNTB) at an absorbance of 412 nm. GSSG was selectively measured after assaying samples in which GSH was masked by pretreatment with 2-vinylpyridine. The difference between the two values gave the GSH level in the cells.

Western Blotting. Cells were collected and lysed with RIPA buffer containing a fresh protease inhibitor mixture (50 μg/mL aprotinin, 0.5 mM phenylmethanesulfonyl fluoride (PMSF), 1 mM sodium orthovanadate, 10 mM NaF, and 10 mM glycerol phosphate). Protein concentrations were quantified using BCA (bicinchoninic acid) assay. Equal amounts of proteins were separated by SDS-PAGE (12%) and electrotransferred onto nitrocellulose membranes. The membranes were blocked with 5% nonfat milk in TBST buffer (20 mM Tris-buffered saline and 0.5% Tween 20) for 1 h at room temperature followed by incubation with the corresponding primary antibodies overnight at 4 °C. After washing with TBST buffer, secondary antibodies were used at 1:2000 dilutions for 45 min at room temperature. Immunoblot proteins were visualized using an enhanced chemiluminescence detection system (Millipore, Germany) followed by exposure to X-ray film. The primary antibodies cathepsin B and glyceraldehyde-3-phosphate dehydrogenase (GAPDH) were used.

Statistical Analysis. Data are presented as mean ± SD for triplicate experiments. The statistical significance of the differences between treated groups and controls was calculated using Student's *t* test. $P < 0.05$ was considered statistically significant.

■ ASSOCIATED CONTENT

Ⓢ Supporting Information

Structure elucidation of compounds **2−20** and **25−36**; ^{1}H and ^{13}C NMR data for compounds **1−20** and **25−36**; X-ray crystallographic structure of **1**; key ^{1}H−^{1}H COSY, HMBC, and NOESY correlations and 1D and 2D NMR, HR-ESI-MS, CD, and IR spectra of compounds **1−20** and **25−36**; ^{1}H and ^{13}C NMR spectra of compounds **45−47**; and a spreadsheet containing SMILES data (CSV). This material is available free of charge via the Internet at http://pubs.acs.org.

■ AUTHOR INFORMATION

Corresponding Author

*Tel: +86-531-8838-2012. Fax: +86-531-8838-2019. E-mail: louhongxiang@sdu.edu.cn.

Author Contributions

§Z.L. and Y.G. contributed equally.

Notes

The authors declare no competing financial interest.

■ ACKNOWLEDGMENTS

This work was financially supported by the National Natural Science Foundation of China (81273383 and 81473107). We acknowledge Prof. M. Li (Shandong University) for providing the fluorescence probe. We are grateful to Dr. Paul E.

DOI: 10.1021/acs.jmedchem.5b00208
J. Med. Chem. XXXX, XXX, XXX−XXX

Floreancig (University of Pittsburgh) for helpful suggestion on the preparation of the manuscript.

■ ABBREVIATIONS USED

SAR, structure−activity relationship; ROS, reactive oxygen species; NAC, *N*-acetylcysteine; MTT, 3-(4,5-dimethylthiazol-2-yl)-2,5-diphenyltetrazolium bromide; IC_{50}, half-maximal inhibitory concentration; SI, selectivity index; DCFH-DA, 2′,7′-dichlorofluorescein diacetate; GSH, glutathione; GSSG, oxidized form of GSH; PBS, phosphate-buffered saline; DMSO, dimethyl sulfoxide; BCA, bicinchoninic acid; BSA, bovine serum albumin; TBST, Tris-buffered saline and Tween 20; SDS-PAGE, sodium dodecyl sulfate polyacrylamide gel electrophoresis

■ REFERENCES

(1) Newman, D. J. Natural products as leads to potential drugs: an old process or the new hope for drug discovery? *J. Med. Chem.* **2008**, *51*, 2589−2599.
(2) Lee, K. H. Discovery and Development of Natural Product-Derived Chemotherapeutic Agents Based on a Medicinal Chemistry Approach. *J. Nat. Prod.* **2010**, *73*, 500−516.
(3) Newman, D. J.; Cragg, G. M. Natural products as sources of new drugs over the 30 years from 1981 to 2010. *J. Nat. Prod.* **2012**, *75*, 311−335.
(4) Asakawa, Y. Chemosystematics of the Hepaticae. *Phytochemistry* **2004**, *65*, 623−669.
(5) Asakawa, Y. Liverworts—potential source of medicinal compounds. *Curr. Pharm. Des.* **2009**, *14*, 3067−3088.
(6) Asakawa, Y.; Ludwiczuk, A.; Nagashima, F. Phytochemical and biological studies of bryophytes. *Phytochemistry* **2013**, *91*, 52−80.
(7) Asakawa, Y.; Ludwiczuk, A.; Nagashima, F. *Chemical Constituents of Bryophytes: Bio- and Chemical Diversity, Biological Activity, and Chemosystematics*; Progress in the Chemistry of Organic Natural Products, Vol. *95*; Springer: Berlin, 2013.
(8) Nagashima, F.; Kondoh, M.; Uematsu, T.; Nishiyama, A.; Saito, S.; Sato, M.; Asakawa, Y. Cytotoxic and apoptosis-inducing *ent*-kaurane-type diterpenoids from the Japanese liverwort *Jungermannia truncata* NEES. *Chem. Pharm. Bull.* **2002**, *50*, 808−813.
(9) Zheng, H.; Chen, Q.; Zhang, M.; Lai, Y.; Lei, L.; Shu, P.; Zhang, J.; Xue, Y.; Luo, Z.; Li, Y.; Yao, G.; Zhang, Y. Cytotoxic *ent*-Kaurane Diterpenoids from *Salvia cavaleriei*. *J. Nat. Prod.* **2013**, *76*, 2253−2262.
(10) Zhan, R.; Li, X. N.; Du, X.; Wang, W. G.; Dong, K.; Su, J.; Li, Y.; Pu, J. X.; Sun, H. D. Bioactive *ent*-Kaurane diterpenoids from *Isodon rosthornii*. *J. Nat. Prod.* **2013**, *76*, 1267−1277.
(11) Sun, H. D.; Huang, S. X.; Han, Q. B. Diterpenoids from *Isodon* species and their biological activities. *Nat. Prod. Rep.* **2006**, *23*, 673−698.
(12) Luo, X.; Pu, J. X.; Xiao, W. L.; Zhao, Y.; Gao, X. M.; Li, X. N.; Zhang, H. B.; Wang, Y. Y.; Li, Y.; Sun, H. D. Cytotoxic *ent*-Kaurane diterpenoids from *Isodon rubescens* var. *lushiensis*. *J. Nat. Prod.* **2010**, *73*, 1112−1116.
(13) Aquila, S.; Weng, Z. Y.; Zeng, Y. Q.; Sun, H. D.; Ríos, J. L. Inhibition of NF-κB activation and iNOS induction by *ent*-kaurane diterpenoids in LPS-stimulated RAW264.7 murine macrophages. *J. Nat. Prod.* **2009**, *72*, 1269−1272.
(14) Zhou, G. B.; Kang, H.; Wang, L.; Gao, L.; Liu, P.; Xie, J.; Zhang, F. X.; Weng, X. Q.; Shen, Z. X.; Chen, J.; Gu, L. J.; Yan, M.; Zhang, D. E.; Chen, S. J.; Wang, Z. Y.; Chen, Z. Oridonin, a diterpenoid extracted from medicinal herbs, targets AML1-ETO fusion protein and shows potent antitumor activity with low adverse effects on t(8;21) leukemia in vitro and in vivo. *Blood* **2007**, *109*, 3441−3456.
(15) Gu, Z. M.; Wu, Y. L.; Zhou, M. Y.; Liu, C. X.; Xu, H. Z.; Yan, H.; Zhao, Y.; Huang, Y.; Sun, H. D.; Chen, G. Q. Pharicin B stabilizes retinoic acid receptor-α and presents synergistic differentiation induction with ATRA in myeloid leukemic cells. *Blood* **2010**, *116*, 5289−5297.
(16) Santagata, S.; Xu, Y.; Wijeratne, E. M. K.; Kontnik, R.; Rooney, C.; Perley, C. C.; Kwon, H.; Clardy, J.; Kesari, S.; Whitesell, L.; Lindquist, S.; Gunatilaka, A. A. L. Using the heat-shock response to discover anticancer compounds that target protein homeostasis. *ACS Chem. Biol.* **2012**, *7*, 340−349.
(17) Wijeratne, E. M. K.; Bashyal, B. P.; Liu, M. X.; Rocha, D. D.; Gunaherath, G. M. K. B.; U'Ren, J. M.; Gunatilaka, M. K.; Arnold, A. E.; Whitesell, L.; Gunatilaka, A. A. L. Geopyxins A−E, *ent*-Kaurane Diterpenoids from Endolichenic Fungal Strains *Geopyxis* aff. *majalis* and *Geopyxis* sp. AZ0066: Structure−Activity Relationships of Geopyxins and Their Analogues. *J. Nat. Prod.* **2012**, *75*, 361−369.
(18) Liu, C. X.; Yin, Q. Q.; Zhou, H. C.; Wu, Y. L.; Pu, J. X.; Xia, L.; Liu, W.; Huang, X.; Jiang, T.; Wu, M. X.; He, L. C.; Zhao, Y. X.; Wang, X. L.; Xiao, W. L.; Chen, H. Z.; Zhao, Q.; Zhou, A. W.; Wang, L. S.; Sun, H. D.; Chen, G. Q. Adenanthin targets peroxiredoxin I and II to induce differentiation of leukemic cells. *Nat. Chem. Biol.* **2012**, *8*, 486−493.
(19) Guo, D. X.; Zhu, R. X.; Wang, X. N.; Wang, L. N.; Wang, S. Q.; Lin, Z. M.; Lou, H. X. Scaparvin A, a novel caged *cis*-clerodane with an unprecedented C-6/C-11 bond, and related diterpenoids from the liverwort *Scapania parva*. *Org. Lett.* **2010**, *12*, 4404−4407.
(20) Wang, L. N.; Zhang, J. Z.; Li, X.; Wang, X. N.; Xie, C. F.; Zhou, J. C.; Lou, H. X. Pallambins A and B, unprecedented hexacyclic 19-nor-secolabdane diterpenoids from the Chinese liverwort *Pallavicinia ambigua*. *Org. Lett.* **2012**, *14*, 1102−1105.
(21) Liu, N.; Li, R. J.; Wang, X. N.; Zhu, R. X.; Wang, L.; Lin, Z. M.; Zhao, Y.; Lou, H. X. Highly oxygenated *ent*-pimarane-type diterpenoids from the Chinese liverwort *Pedinophyllum interruptum* and their allelopathic activities. *J. Nat. Prod.* **2013**, *76*, 1647−1653.
(22) Lin, Z. M.; Guo, Y. X.; Wang, S. Q.; Wang, X. N.; Chang, W. Q.; Zhou, J. C.; Yuan, H.; Lou, H. Diterpenoids from the Chinese liverwort *Heteroscyphus tener* and their antiproliferative effects. *J. Nat. Prod.* **2014**, *77*, 1336−1344.
(23) Zhang, D. Y.; Tang, Y.; Wang, K.; Wu, X. M.; Hua, W. Y. Synthesis and antitumor activity of *ent*-kaurane diterpenoids. *J. China Pharm. Univ.* **2010**, *41*, 20−25.
(24) Nagashima, F.; Kasai, W.; Kondoh, M.; Fujii, M.; Watanabe, Y.; Braggins, J. E.; Asakawa, Y. New *ent*-kaurene-type diterpenoids possessing cytotoxicity from the New Zealand liverwort *Jungermannia* species. *Chem. Pharm. Bull.* **2003**, *51*, 1189−1192.
(25) Nagashima, F.; Kondoh, M.; Fujii, M.; Takaoka, S.; Watanabe, Y.; Asakawa, Y. Novel cytotoxic kaurane-type diterpenoids from the New Zealand liverwort *Jungermannia* species. *Tetrahedron* **2005**, *61*, 4531−4544.
(26) Qu, J. B.; Zhu, R. L.; Zhang, Y. L.; Guo, H. F.; Wang, X. N.; Xie, C. F.; Yu, W. T.; Ji, M.; Lou, H. X. *ent*-Kaurane diterpenoids from the liverwort *Jungermannia atrobrunnea*. *J. Nat. Prod.* **2008**, *71*, 1418−1422.
(27) Trachootham, D.; Lu, W.; Ogasawara, M. A.; Nilsa, R. D.; Huang, P. Redox regulation of cell survival. *Antioxid. Redox Signaling* **2008**, *10*, 1343−1374.
(28) Rhee, S. G. H_2O_2, a necessary evil for cell signaling. *Science* **2006**, *312*, 1882−1883.
(29) Dickinson, B. C.; Chang, C. J. Chemistry and biology of reactive oxygen species in signaling or stress responses. *Nat. Chem. Biol.* **2011**, *7*, 504−511.
(30) Alexandre, J.; Batteux, F.; Nicco, C.; Chéreau, C.; Laurent, A.; Guillevin, L.; Weill, B.; Goldwasser, F. Accumulation of hydrogen peroxide is an early and crucial step for paclitaxel-induced cancer cell death both in vitro and in vivo. *Int. J. Cancer* **2006**, *119*, 41−48.
(31) Trachootham, D.; Zhou, Y.; Zhang, H.; Demizu, Y.; Chen, Z.; Pelicano, H.; Chiao, P. J.; Achanta, G.; Arlinghaus, R. B.; Liu, J.; Huang, P. Selective killing of oncogenically transformed cells through a ROS-mediated mechanism by β-phenylethyl isothiocyanate. *Cancer Cell* **2006**, *10*, 241−252.
(32) Trachootham, D.; Alexandre, J.; Huang, P. Targeting cancer cells by ROS-mediated mechanisms: a radical therapeutic approach? *Nat. Rev. Drug Discovery* **2009**, *8*, 579−591.

DOI: 10.1021/acs.jmedchem.5b00208
J. Med. Chem. XXXX, XXX, XXX−XXX

(33) Gorrini, C.; Harris, I. S.; Mak, T. W. Modulation of oxidative stress as an anticancer strategy. *Nat. Rev. Drug Discovery* **2013**, *12*, 931−947.
(34) Zhen, T.; Wu, C. F.; Liu, P.; Wu, H. Y.; Zhou, G. B.; Lu, Y.; Liu, J. X.; Liang, Y.; Li, K. K.; Wang, Y. Y.; Xie, Y. Y.; He, M. M.; Cao, H. M.; Zhang, W. N.; Chen, L. M.; Petrie, K.; Chen, S. J.; Chen, Z. Targeting of AML1-ETO in t(8;21) leukemia by oridonin generates a tumor suppressor-like protein. *Sci. Transl. Med.* **2012**, *4*, No. 127ra38.
(35) Huang, J.; Wu, L.; Tashiro, S.; Onodera, S.; Ikejima, T. Reactive oxygen species mediate oridonin-induced HepG2 apoptosis through p53, MAPK, and mitochondrial signaling pathways. *J. Pharmacol. Sci.* **2008**, *107*, 370−379.
(36) Yu, Z. Y.; Liang, Y. G.; Xiao, H.; Shan, Y. J.; Dong, B.; Huang, R.; Fu, Y. L.; Zhao, Z. H.; Liu, Z. Y.; Zhao, Q. S.; Wang, S. Q.; Chen, J. P.; Mao, B. Z.; Cong, Y. W. Melissoidesin G, a diterpenoid purified from *Isodon melissoides*, induces leukemic-cell apoptosis through induction of redox imbalance and exhibits synergy with other anticancer agents. *Int. J. Cancer* **2007**, *121*, 2084−2094.
(37) Liao, Y. J.; Bai, H. Y.; Li, Z. H.; Zou, J.; Chen, J. W.; Zheng, F.; Zhang, J. X.; Mai, S. J.; Zeng, M. S.; Sun, H. D.; Pu, J. X.; Xie, D. Longikaurin A, a natural *ent*-kaurane, induces G2/M phase arrest via downregulation of Skp2 and apoptosis induction through ROS/JNK/c-Jun pathway in hepatocellular carcinoma cells. *Cell Death Dis.* **2014**, *5*, No. e1137.
(38) Dickinson, D. A.; Forman, H. J. Cellular glutathione and thiols metabolism. *Biochem. Pharmacol.* **2002**, *64*, 1019−1026.
(39) Chatterjee, A. Reduced glutathione: a radioprotector or a modulator of DNA-repair activity? *Nutrients* **2013**, *5*, 525−542.
(40) Lu, S. C. Regulation of glutathione synthesis. *Mol. Aspects Med.* **2009**, *30*, 42−59.
(41) Li, W.; Sun, W.; Yu, X.; Du, L.; Li, M. Coumarin-based fluorescent probes for H_2S detection. *J. Fluoresc.* **2013**, *23*, 181−186.
(42) Yuan, L.; Jian, W.; Zhang, D.; Aubry, A. F.; Arnold, M. E. Application of a stabilizer cocktail of *N*-ethylmaleimide and phenylmethanesulfonyl fluoride to concurrently stabilize the disulfide and ester containing compounds in a plasma LC−MS/MS assay. *J. Pharm. Biomed. Anal.* **2014**, *88*, 552−561.
(43) Kim, J. A.; Kang, Y. S.; Park, S. H.; Kim, H. W.; Cho, S. Y.; Lee, Y. S. Role of reactive oxygen species in apoptosis induced by *N*-ethylmaleimide in HepG2 human hepatoblastoma cells. *Eur. J. Pharmacol.* **2001**, *433*, 1−6.
(44) Yellaturu, C. R.; Bhanoori, M.; Neeli, I.; Rao, G. N. *N*-Ethylmaleimide Inhibits Platelet-Derived Growth Factor BB-Stimulated Akt Phosphorylation via Activation of Protein Phosphatase 2A. *J. Biol. Chem.* **2002**, *277*, 40148−40155.
(45) Rajendran, L.; Knölker, H. J.; Simons, K. Subcellular targeting strategies for drug design and delivery. *Nat. Rev. Drug Discovery* **2010**, *9*, 29−42.
(46) Mohamed, M. M.; Sloane, B. F. Cysteine cathepsins: multifunctional enzymes in cancer. *Nat. Rev. Cancer* **2006**, *6*, 764−775.
(47) Mizushima, N.; Levine, B.; Cuervo, A. M.; Klionsky, D. J. Autophagy fights disease through cellular self-digestion. *Nature* **2008**, *451*, 1069−1075.
(48) Boya, P.; Kroemer, G. Lysosomal membrane permeabilization in cell death. *Oncogene* **2008**, *27*, 6434−6451.
(49) Sheldrick, G. M.; Schneider, T. R. *Methods Enzymol.* **1997**, *277*, 319−343.
(50) Griffith, O. W. Determination of glutathione and glutathione disulfide using glutathione reductase and 2-vinylpyridine. *Anal. Biochem.* **1980**, *106*, 207−212.

DOI: 10.1021/acs.jmedchem.5b00208
J. Med. Chem. XXXX, XXX, XXX−XXX